Energy Geoscience xxx (xxxx) xxx

Contents lists available at ScienceDirect

Energy Geoscience

journal homepage: www.keaipublishing.com/en/journals/energy-geoscience

Geochemistry and hydrocarbon source rock potential of shales from the Palaeo-Mesoproterozoic Vindhyan Supergroup, central India

Arvind Kumar Singh [a], Partha Pratim Chakraborty [b, c, *]

[a] Birbal Sahni Institute of Palaeosciences, 53 University Road, Lucknow, 226007, India
[b] Department of Geology, University of Delhi, New Delhi, 110007, India
[c] Hiroshima Institute of Plate Convergence Region Research, Hiroshima University, Higashi−Hiroshima, 7398526, Japan

ARTICLE INFO

Article history:
Received 30 June 2021
Received in revised form
5 October 2021
Accepted 18 October 2021

Keywords:
Shale geochemistry
Provenance
Organic matter
Hydrocarbon potential
Vindhyan basin

ABSTRACT

With increase in shale gas exploration, inorganic and organic geochemical investigations of shale have become extremely important. Here, we explore the six argillaceous (shale) intervals (Arangi, Koldaha, Rampur, Bijaygarh, Rewa and Sirbu shale) from Son valley sector, Vindhyan Basin with an aim to understand provenance conditions, palaeoclimate, tectonic setting and hydrocarbon generation potential. Whole rock geochemistry indicates Vindhyan sediments derived from felsic source(s) except for Sirbu shale that indicates additional influx of mafic rocks with differentiated felsic source. A comparative study of Vindhyan shale rare earth elements (REEs) points to Mahakoshals and Chhotanagpur gneissic complex (CGC) as probable sediment provenance for Vindhyan sediments. CIA analysis, after necessary corrections for K-metasomatism, suggests evolution in weathering and palaeoclimate indicating a transformation from moderate weathering conditions with warm and humid climate during lower Vindhyan deposition to intense weathering conditions with hot and humid climate during upper Vindhyan deposition. Trace (La/Y *vs.* Sc/Cr) and REE analysis indicates passive margin setting for Vindhyan sediments whereas a wide range spanning passive to active continental margin setting is also inferred using (Th-Sc-Zr/10) and (Th−La-Sc) ternary diagrams. However, these tectonic discriminant diagrams lack in explaining rift- or sag-related origin of any intracratonic basin such as the Vindhyan Basin. The total organic carbon (TOC) content in Vindhyan shales ranges from 0.29% to 8.44%. The thermally liberated hydrocarbon (S_1) values range from 0.01 to 0.18 mg HC/g rock (milligram hydrocarbon per gram of rock sample), whereas hydrocarbon from cracking of the kerogen (S_2) shows values ranging from 0.04 to 0.47 mg HC/g rock. Based on modified Van Krevelen correlation (HI *vs.* T_{max}) diagram, organic matter from Arangi and Bijaygarh shales is characterized as thermally mature, Type III kerogen of gas prone character indicating good to very good gas generation potential.

1. Introduction

Shale, the most abundant rock among clastic sediments worldwide (>70% of sediment cover), is a fissile, thinly laminated, fine grained clastic sedimentary rock that are formed under a specific set of sedimentological, palaeoclimatic, palaeoecological and geochemical conditions (Wignall, 1994; Tyson 2004; Schieber, 2011; Bose et al., 2012; Hu et al., 2020). The geochemistry of shale including trace elements and REE in particular, represents the average crustal composition of upper continental crust and is considered an excellent proxy of provenance, tectonics or palaeoclimate interpretation (Nesbitt and Young, 1982; Roser and Korsch, 1988; Fu et al., 2010; Li et al., 2012). While rapid alteration of feldspar and leaching of accessory minerals in sandstones often result in erroneous interpretation of provenance (Blatt, 1985), the impermeable character of fine grained clastics enforces elemental retention and preservation of original signatures of

* Corresponding author. Department of Geology, University of Delhi, New Delhi, 110007, India.
E-mail address: parthageology@gmail.com (P.P. Chakraborty).

Production and Hosting by Elsevier on behalf of KeAi

https://doi.org/10.1016/j.engeos.2021.10.007

Please cite this article as: A.K. Singh and P.P. Chakraborty, Geochemistry and hydrocarbon source rock potential of shales from the Palaeo-Mesoproterozoic Vindhyan Supergroup, central India, Energy Geoscience, https://doi.org/10.1016/j.engeos.2021.10.007

source rocks and their diagenetic changes. Also, sequestration and stability of organic matter makes shales an efficient sink for long-term carbon cycle (Basu et al., 2019) and a prospective hydrocarbon source rock. Multidisciplinary studies in the last one and half decade have allowed workers to recognize, hitherto undescribed, distribution and composition of hydrocarbon generating organic matter in the Precambrian rock record. From documentation of black shales in the Precambrian, their Chemical Index of Alteration (CIA) peaks, black shale/total shale ratio and their correlation with $\delta^{13}C$ values of contemporary marine carbonates, Condie et al. (2001) suggested higher rates of organic carbon buried in the late Palaeoproterozoic-Mesoproterozoic (2–1.6 Ga) with less prominent peaks in the late Archean (2.7–2.5 Ga) and the late Neoproterozoic (800–600 Ma) time. The discovery of giant oil and gas fields of the Precambrian in Canada, Oman and Russia (Craig et al., 2013) has enhanced the interest on studies related to Precambrian shales as untapped hydrocarbon resources.

Unlike the Phanerozoic, the Proterozoic shales dominantly were deposited in storm-dominated shallow marine epicontinental shelves for which there is little modern analog (Trabucho-Alexandre, 2015; Ghosh et al., 2016). The deposition of various types of shales (green, yellow, red, grey and black) with varied sand/silt content is attributed to a wide range of basin bathymetry, depositional environment, processes, terrestrial supply, sea level fluctuations, water column chemistry and organic matter content (Bose et al., 2001; Cullers, 2002; Kasanzu et al., 2008; Algeo and Tribovillard, 2009; Fu et al., 2010; Armstrong-Altrin et al., 2013). With growing interest in the Proterozoic shales (Zhu et al., 2018), it is necessary to explore shales present in Indian Proterozoic basins. The Palaeo-Mesoproterozoic Vindhyan Supergroup (>1631 ± 5 Ma) (Ray et al., 2002 to 1000 Ma; Malone et al., 2008), central India with multiple stratigraphic intervals of argillaceous sediments in its lithosuccession, has become a natural target for probe. Occurrence of organic-rich black shales, algal laminites and stromatolitic limestones as a significant part of the basin succession attracted workers for decades (Chakraborty, 2004; Banerjee et al., 2006; Dutta et al., 2006; Sharma and Shukla, 2009; Sharma et al., 2009; Singh and Chakraborty, 2020). Such types of Proterozoic rocks with high organic carbon content have yielded commercial hydrocarbons in other Proterozoic basins of the world (Hunt, 1996; Cozzi et al., 2012; Craig et al., 2013) including the report of oldest live oil from the Mesoproterozoic (1417 ± 29 Ma) Velkerri Formation, Roper Group, Australia. It is believed that rift-to-sag tectonics with discrete episodic subsidence and development of entrapment condition in the Vindhyan Basin would be favourable for the accumulation of organic-rich sediments with hydrocarbon generation potential (Bose et al., 2001; Dayal et al., 2014). Taking this into consideration, the Directorate General of Hydrocarbons (DGH), Govt. of India in 2012 categorized the basin as hydrocarbon prospective under category III sedimentary basin of India that has led to an increased interest for assessment of the Vindhyan Basin in terms of spatial and temporal distribution of organic carbon-rich horizons, characterization of organic matter, their degree of maturation and source rock potential.

Against this backdrop, it may be significant to underline that except for depositional process, environment, and basin tectonics studies (Chakrabarti et al., 2007; Paikaray et al., 2008; Raza et al., 2010, 2012; Shukla et al., 2020), the Vindhyan Basin is seldom attended in terms of shale geochemistry (both inorganic and organic), especially in the context of provenance, its weathering history, palaeoclimate, basin tectonics and hydrocarbon source rock potential (Banerjee et al., 2006; Dayal et al., 2014; Sinha et al., 2017). Geochemical studies, whenever attempted, remained confined within some specific stratigraphic intervals and hence, fell short of providing a holistic idea on the evolution of provenance and changes in biogeochemical character, if any through the >500 Ma depositional history of the basin. Here, we attempt a whole rock geochemistry (major, trace and REE) and evaluation of organic matter from outcrop shale samples of all six argillaceous intervals (Arangi, Koldaha, Rampur, Bijaygarh, Rewa and Sirbu) present within the Vindhyan Supergroup, exposed at the Son valley, central India. We intend to provide an idea on the nature of provenance and its scale of weathering, palaeoclimatic condition and nature of organic matter (source and thermal maturity) including hydrocarbon potential.

2. Geological background

Indian cratonic sedimentary basins are comparable with the Proterozoic basins of Australia, North America and the Siberian platform with respect to size, sediment thickness, depositional systems, age and duration of basin history (Patranabis Deb, 2004; Wani and Mondal, 2011). Strong evidences suggest that their initiation and closing are connected to break-up and assembly of supercontinents Kenorland, Columbia and Rodinia (Basu and Bickford, 2015; Chakraborty et al., 2020). The Vindhyan Basin, formed within the Bundelkhand craton (3.3-2.5 Ga) (Crawford and Compston, 1970; Mondal et al., 2002), covers an exposed area of over 178,000 km^2 with approximately 4500 m thick siliciclastic-carbonate package of mildly deformed and unmetamorphosed sediments (Tandon et al., 1991; (Fig. 1). The Aravalli-Delhi fold belt (2500-900 Ma) (Roy, 1988) demarcates the basin in its west while the Satpura orogen (1600–850 Ma) (Verma, 1991) bounds it in the south and east. The Bundelkhand granite massif, occurring at the center of the basin, divides the basin into two sub-basins—the Son Valley Vindhyans to the east and the Rajasthan Vindhyans to the west. Majority of the northern part of the basin is overlain by recent alluvium from the Gangetic plain while the southern part is covered by Deccan lava (the Cretaceous to Oligocene) (Krishnan, 1968). Rifting in the Aravalli-Bundelkhand craton at around 2.5 Ga (Eriksson et al., 1999; Meert et al., 2010), reduced the cratonic thickness and led to accumulation of the Palaeoproterozoic sediments within rift-bound Gwalior, Bijawar and Mahakoshal Basins (Mazumder et al., 2000; Bose et al., 2001; Chakraborty et al., 2015). Unconformably overlying the rift-guided Palaeoproterozoic sediment successions, the mildly deformed late Palaeoproterozoic-Mesoproterozoic Vindhyan Supergroup were deposited as a mixed siliciclastic-carbonate rich sediment package in its lower part and siliciclastics dominated package in the upper part. The basin succession is subdivided into two Groups namely the Lower Vindhyan (Semri Group) and the Upper Vindhyan Group (Kaimur, Rewa and Bhander Groups) by a basin wide unconformity and its correlative conformity (Bose et al., 2015; Mandal et al., 2019) (Fig. 1b). Here in the follow-up discussion, we have referred to the Arangi, Koldaha and Rampur shales as the lower Vindhyan shales, belonging to the Semri Group, and Bijaygarh, Rewa and Sirbu shale successions together as the upper Vindhyan shales, belonging to Kaimur, Rewa and Bhander Groups.

3. Materials and methods

3.1. Sampling

Analyses of major, trace, REE, TOC content and measurements of various hydrocarbon indices (S_1, S_2) were carried out on samples collected from all six different shale formations (Arangi, Koldaha, Rampur, Bijaygarh, Rewa and Sirbu) from the Vindhyan succession exposed in the Son valley. The outcrop section of shale was hammered, scoured and scratched for exposing fresh shale samples and in total, seventy-five whole rock samples encompassing six

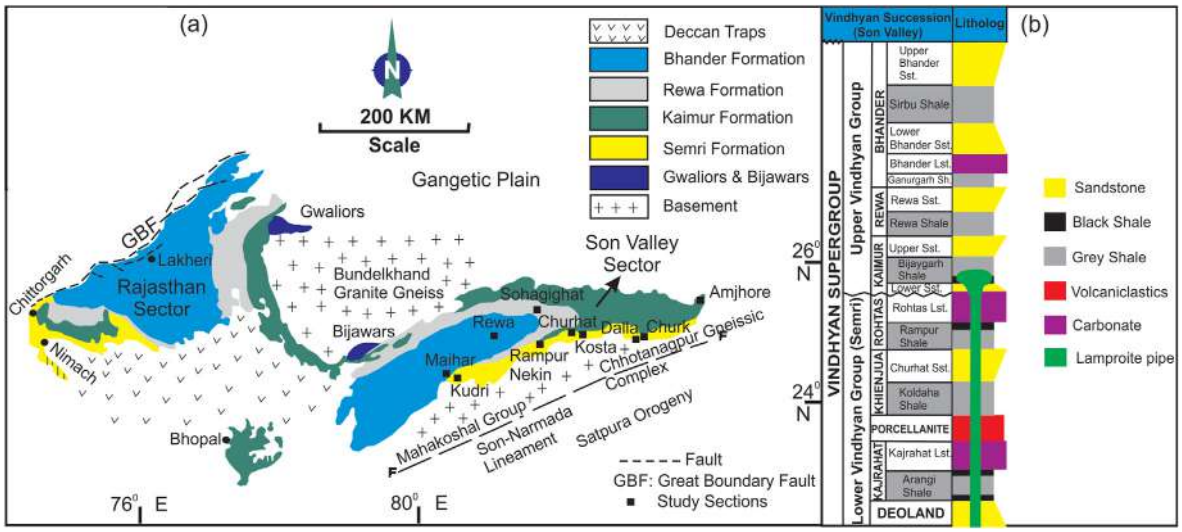

Fig. 1. (a) Geological map of the Vindhyan Basin (modified after Krishnan and Swaminath, 1959) showing study area locations in the Son valley sector; (b) Stratigraphy of the Vindhyan Supergroup exposed at the Son valley highlighting the studied shale intervals (grey).

different shale horizons from lower and upper Vindhyan were collected. The small chips of samples were washed and carefully processed with distilled water for removing any weathering rinds and dried at room temperature to remove any oxidized part. Air dried chips were powdered to 200 mesh and oven dried at 80 °C for 2 h before storing in a desiccator for geochemical analyses. For organic geochemical analyses, chips were powdered with agate mortar.

3.2. X-ray fluorescence (XRF) analysis

Sample pellets were analyzed for major elements using Siemens SRS 3000 WD-XRF spectrometer at Wadia Institute of Himalayan Geology, Dehradun and Panalytical Axio fast WD-XRF spectrometer at National Geophysical Research Institute (NGRI), Hyderabad, India. The precession level of major oxide data is better than 1.5%. Analytical techniques, accuracy and precision of the instruments are described in Saini et al. (1998). The international shale rock standards used for calibrations are GSR-5, SGR-1, SDO-1 and SCHS-1.

3.3. Inductively coupled plasma mass spectrometry (ICP-MS) analysis

Vindhyan shale samples were analyzed for trace elements and REE using an inductively coupled plasma mass spectrometry (ICP-MS; PerkinElmer SCIEXELAN DRC-e quadrupole) at geochemistry divisions of Wadia Institute of Himalayan Geology, Dehradun and National Geophysical Research Institute, Hyderabad, India. A total of 50 mg of powered samples were digested with 10 ml of 7:3:1 HF–HNO_3–$HClO_4$ acid mixture in high pressure PTE vessels at 150 °C for 48 h. Then the mixture was openly heated to dryness at 180 °C to form crystalline paste. The solid precipitate in each PTE vessels were dissolved by adding 20 ml of 1:1 HNO_3-ultrapure water mixture and heated at 80 °C for 1 h. The precision of ICP-MS trace-element and REE data is better than 5%. The details of the analytic techniques and accuracy of the instrument are further discussed in Roy et al. (2007).

3.4. TOC analysis

The TOC content of shale samples were analyzed using total organic carbon analyzer (Shimadzu TOC-$L_{CPH/CPN}$) with attached Solid Sample module (SSM-5000A) at Chemical Sedimentology Lab, Department of Geology, University of Delhi, India. It adopts combustion catalytic oxidation method at 680 °C in which powdered samples (20 mg for each) were oxidized using SSM and, CO_2 then generated was directed to NDIR detector with TOC-L instrument for analysis. The samples were heated to 900 °C for total carbon (TC) and 200 °C for inorganic carbon (IC) concentrations. TOC values were calculated using formula [TOC = TC-IC].

3.5. Rock-Eval pyrolysis

A total of 19 freshly powdered shale samples (50–70 mg for each) were analyzed for contents of free volatile/light hydrocarbons (S_1), heavy hydrocarbons generated with thermal cracking of Kerogen (S_2), Oxygen index (OI), Hydrogen index (HI) and T_{max} using Rock-Eval 6 (Turbo version) at Department of Earth Science, Indian Institute of Technology, Mumbai, India. Samples were pyrolyzed in an inert atmosphere and further residual carbon was burnt in an oxidation oven. Flame Ionization Detector (FID) was used for detection of released hydrocarbon during pyrolysis and on-line infra-red detection were used to measure released CO and CO_2. Pyrolysis was carried out at a temperature range of 300°C–650 °C at a rate of 25 °C/min (cf. Lafargue et al., 1998). Oxidation started at 300 °C and followed by an increase of temperature up to 750 °C with a temperature gradient 25 °C/min in order to burn all residual carbon.

4. Results

4.1. Major element geochemistry

Significant fluctuations are recorded in the abundance of major element concentrations of lower and upper Vindhyan shales (Table 1). SiO_2 concentration in Vindhyan shales varies from 51 to 87 wt% with an average of 64.97 wt%. Wide variations can also be observed in Al_2O_3 (7.07–23.53 wt%) and K_2O content (1.60–5.44 wt

Table 1
Major element concentrations (wt%) of Vindhyan shales with calculated CIA values.

Shales	SiO_2	TiO_2	Al_2O_3	Fe_2O_3	MgO	MnO	CaO	Na_2O	K_2O	P_2O_5	LOI	Total	CIA
Sirbu shale													
N1/28	63.81	0.76	17.44	4.93	1.64	0.02	0.60	0.51	3.37	0.22	5.24	93.30	80
N2/28	65.36	0.75	16.71	5.09	1.61	0.07	0.50	0.58	3.03	0.11	4.81	93.81	80
N3/28	72.45	0.61	12.74	4.13	1.29	0.08	0.63	0.77	2.02	0.07	3.31	94.79	79
N4/28	67.98	0.67	15.32	4.69	1.45	0.05	0.52	0.61	2.72	0.08	4.59	94.09	80
N5/28	69.58	0.56	14.83	4.19	1.42	0.02	0.48	0.51	2.61	0.05	4.22	94.25	80
N6/28	59.47	0.74	19.74	5.39	1.64	0.03	0.66	0.29	4.30	0.30	6.72	92.56	80
N7/28	68.12	0.63	17.38	3.19	1.16	0.01	0.47	0.51	2.94	0.07	4.62	94.48	82
N8/28	63.91	0.67	17.62	4.93	1.83	0.05	0.63	0.51	3.40	0.19	4.83	93.74	80
N9/28	66.41	0.66	16.83	4.33	1.62	0.02	0.52	0.58	3.06	0.08	4.79	94.11	80
N10/28	69.25	0.59	15.16	4.10	1.45	0.06	0.49	0.64	2.72	0.07	4.17	94.53	80
SS1	70.68	0.57	14.81	3.66	1.30	0.02	0.55	0.57	2.48	0.10	3.61	94.74	80
SS2	64.57	0.66	17.19	4.60	1.58	0.02	0.65	0.37	3.20	0.08	5.31	92.92	81
SS3	61.11	0.73	19.47	5.21	1.78	0.02	0.55	0.31	4.14	0.05	6.24	93.37	80
SS4	64.91	0.70	17.57	4.56	1.64	0.02	0.53	0.44	3.21	0.05	4.93	93.63	81
SS5	62.38	0.72	18.65	5.34	1.81	0.03	0.54	0.34	3.79	0.08	5.89	93.68	81
SBS3	63.97	0.68	17.98	4.68	1.75	0.02	0.53	0.60	3.60	0.06	4.93	93.87	79
SBS4	63.37	0.66	18.01	4.83	1.76	0.02	0.55	0.59	3.51	0.05	4.91	93.35	79
SBS5	64.73	0.64	17.51	4.70	1.60	0.04	0.56	0.64	3.24	0.06	4.47	93.72	80
SBS6	63.71	0.70	17.85	4.97	2.03	0.04	0.48	0.69	3.64	0.09	4.23	94.20	79
SBS7	63.95	0.72	17.87	4.70	1.77	0.02	0.51	0.55	3.78	0.04	5.08	93.91	79
SBS8	66.58	0.65	16.55	4.57	1.68	0.03	0.50	0.65	3.23	0.04	4.55	94.48	79
SBS9	61.71	0.69	19.14	5.04	1.77	0.03	0.56	0.52	4.04	0.07	5.43	93.57	79
SBS10	66.39	0.62	16.94	4.10	1.57	0.02	0.51	0.62	3.10	0.05	4.28	93.92	80
Avg.	65.41	0.67	17.10	4.61	1.62	0.03	0.54	0.54	3.27	0.09	4.83	93.87	80
Rewa shale													
PS1	68.39	0.72	15.30	4.43	2.00	0.01	0.57	0.18	5.10	0.12	3.15	96.83	74
PS2	64.31	0.83	12.66	5.77	2.07	0.14	2.79	0.12	4.65	0.31	6.26	93.65	72
PS3	65.97	1.04	17.46	4.67	1.29	0.01	0.56	0.22	5.01	0.17	4.52	96.41	76
PS4	65.49	0.96	17.94	4.75	1.54	0.00	0.58	0.16	5.28	0.10	4.65	96.78	76
PS5	60.30	1.25	23.53	5.92	0.47	0.02	0.60	0.09	4.89	0.09	5.71	97.17	82
PS6	58.94	1.24	22.90	7.75	0.71	0.02	0.66	0.08	5.00	0.11	5.75	97.42	82
JS1	61.13	1.27	18.43	8.52	0.86	0.02	0.64	0.13	5.01	0.13	4.51	96.15	78
Avg.	63.50	1.04	18.32	5.97	1.28	0.03	0.91	0.14	4.99	0.15	4.94	96.34	77
Bijaygarh shale													
BGS1	65.36	0.73	10.90	12.78	0.76	0.01	0.12	0.07	3.16	0.33	5.30	94.22	77
BGS2	58.79	0.80	10.84	20.73	0.85	0.01	0.19	0.07	3.24	0.43	4.22	95.95	76
BGS3	59.23	0.76	10.68	21.98	0.77	0.01	0.11	0.09	3.14	0.35	1.88	97.12	76
BGS4	66.44	0.74	11.07	11.87	0.78	0.01	0.13	0.09	3.42	0.35	5.24	94.90	75
BGS5	64.23	0.72	11.48	14.53	0.76	0.02	0.12	0.08	3.22	0.34	4.50	95.50	77
BGS6	61.67	0.81	11.86	18.33	0.66	0.01	0.14	0.07	3.12	0.38	2.95	97.05	78
BGS7	60.24	0.87	10.81	19.39	0.77	0.01	0.10	0.06	3.09	0.31	5.51	95.65	77
Avg.	62.28	0.78	11.09	17.09	0.76	0.01	0.13	0.08	3.20	0.36	4.23	95.77	77
Rampur shale													
RN1	66.38	0.72	13.81	5.25	2.12	0.01	1.13	0.06	4.94	0.22	4.96	94.65	73
RN2	56.56	0.39	7.95	4.52	6.44	0.04	6.33	0.04	4.76	0.19	13.40	87.22	62
RN3	61.59	0.52	10.74	4.63	3.73	0.03	3.55	0.07	5.03	0.20	10.30	90.09	68
RN4	69.97	0.60	11.99	5.02	2.40	0.01	0.69	0.06	5.00	0.21	3.48	95.95	70
BS1	51.44	0.31	7.07	4.36	6.37	0.03	12.50	0.03	4.81	0.15	11.98	87.08	59
BS2	67.59	0.71	13.90	5.27	2.12	0.01	0.68	0.07	5.26	0.25	3.80	95.86	72
BS3	61.34	0.58	11.27	5.63	3.28	0.03	3.16	0.05	4.90	0.25	9.23	90.48	69
RS1	63.08	0.79	17.75	6.76	1.62	0.02	0.57	0.04	5.07	0.09	5.28	95.78	78
RS2	62.57	0.83	19.16	6.77	1.46	0.01	0.56	0.04	5.09	0.08	4.41	96.57	79
RS3	62.46	0.82	18.18	6.83	1.48	0.01	0.61	0.04	5.16	0.10	3.70	95.68	78
Avg.	62.30	0.63	13.18	5.50	3.10	0.02	2.98	0.05	5.00	0.17	7.05	92.94	71
Koldaha shale													
KSK1	59.22	0.78	14.75	7.38	1.78	0.10	2.12	0.31	4.64	0.11	8.47	91.20	74
KSK2	61.90	0.89	16.70	7.94	1.32	0.03	0.62	0.24	4.71	0.11	5.31	94.46	76
KSK3	61.56	0.89	16.89	7.99	1.30	0.04	0.66	0.26	4.76	0.09	4.34	94.44	76
KSK4	62.21	0.91	16.97	7.86	1.30	0.02	0.62	0.23	4.74	0.11	4.14	94.97	77
KSK5	63.68	0.83	15.58	7.08	1.66	0.03	0.66	0.40	4.68	0.11	3.45	94.71	74
KS1	65.47	0.62	15.45	5.88	2.09	0.03	0.75	0.51	4.66	0.11	4.29	95.57	73
KS2	65.13	0.90	15.57	6.25	1.55	0.04	0.72	1.05	4.55	0.15	3.96	95.90	71
KS3	65.10	0.89	15.39	6.26	1.57	0.06	0.73	0.93	4.55	0.14	4.25	95.62	71
KS4	63.76	0.92	15.89	6.59	1.49	0.03	0.68	0.76	4.59	0.13	4.61	94.83	72
GS1	62.53	0.53	15.76	6.49	3.13	0.05	0.80	0.52	4.34	0.08	4.68	94.23	75
GS2	61.80	0.54	16.04	6.70	3.04	0.03	0.97	0.39	4.41	0.07	4.94	93.99	76
GS3	63.09	0.53	16.67	6.68	2.56	0.02	0.62	0.30	4.72	0.07	5.33	95.26	76
GS4	63.45	0.52	16.28	6.57	2.70	0.02	0.56	0.33	4.65	0.07	4.66	95.15	75
GS5	63.10	0.50	15.98	6.51	2.83	0.04	0.77	0.37	4.62	0.07	4.52	94.79	75
GS6	63.20	0.53	16.07	6.38	2.81	0.02	0.61	0.40	4.68	0.06	4.62	94.76	75
GS7	62.42	0.54	16.39	6.19	2.80	0.02	0.56	0.32	5.01	0.07	4.81	94.32	74
GS8	63.36	0.54	15.99	6.30	2.96	0.02	0.64	0.39	4.46	0.08	4.92	94.74	75
KDS0	62.45	0.51	16.02	7.01	2.83	0.03	0.57	0.17	5.22	0.08	4.95	94.89	74

Table 1 (*continued*)

Shales	SiO_2	TiO_2	Al_2O_3	Fe_2O_3	MgO	MnO	CaO	Na_2O	K_2O	P_2O_5	LOI	Total	CIA
KDS1	62.92	0.53	16.45	5.68	2.26	0.02	0.62	0.17	5.44	0.07	5.21	94.16	74
KDS2	64.55	0.52	15.86	5.35	2.43	0.02	0.60	0.18	5.34	0.07	4.48	94.92	74
KDS3	63.75	0.54	15.54	5.00	2.41	0.01	0.58	0.18	5.37	0.08	4.07	93.46	73
Avg.	63.08	0.66	16.01	6.58	2.23	0.03	0.74	0.40	4.77	0.09	4.76	94.59	74
Arangi shale													
B31	86.89	0.27	7.95	0.76	0.36	0.001	0.18	0.12	3.44	0.03	–	100	68
B32	78.57	0.46	12.76	1.06	1.63	0.003	0.13	0.20	5.19	0.01	–	100	70
B34	87.83	0.35	9.13	0.48	0.52	0.002	0.02	0.04	1.60	0.04	–	100	80
B35	87.17	0.32	8.46	0.85	0.48	0.002	0.05	0.06	2.55	0.06	–	100	76
Avg.	85.11	0.35	9.57	0.79	0.75	0.00	0.09	0.10	3.19	0.04	–	100	74

%) with their averages being 15.36 wt% and 4.13 wt% respectively. A high K_2O content (more than Avg. PAAS value of 3.68%) (Taylor and McLennan, 1985) may be due to potash metasomatism, and an anomalous high Fe_2O_3 content (21.98) in Bijaygarh shale may be because of pyrite occurrence. The upper Vindhyan shales exhibit higher TiO_2 content (0.56–1.27 wt%) compared to that of lower Vindhyan shales (0.27–0.92 wt%). An increase in the average concentrations of Al_2O_3 (14.5–16.2 wt%) and TiO_2 (0.61–0.76 wt%) is recorded from lower to upper Vindhyan shales. The higher Al_2O_3 and TiO_2 contents commonly indicate higher degree of chemical weathering in the provenance.

The shales are classified following Herron (1988) which is considered beneficial for the classification of clastic sedimentary rocks (Roddaz et al., 2006; Kasanzu et al., 2008). On the SiO_2/Al_2O_3 *vs.* Fe_2O_3/K_2O chemical classification diagram, Vindhyan shales mostly plot in the field of shale except for the Arangi and Bijaygarh shales. The Bijaygarh shale samples plot in the field of 'Fe-Shale' because of high diagenetic pyrite content (cf. Sarkar et al., 2010) whereas few Arangi and Rampur shale samples are classified as 'Arkose' and 'Wackes' due to their high K_2O and low Fe_2O_3 contents (Fig. 2a). The Vindhyan shales, in general, display low SiO_2/Al_2O_3 ratio (4.2) and high K_2O/Na_2O ratio (31.43). Understandably, these ratios are highly susceptible to fractionation of quartz, albite and illite during sediment sorting process. A dominance of clay minerals in the shale composition is ascertained from variation of SiO_2/Al_2O_3 with respect to K_2O/Na_2O (Fig. 2b) (Wronkiewicz and Condie, 1987; Deru et al., 2007). The low K_2O/Al_2O_3 ratio (Avg. < 0.3) also corroborate clay domination in primary mineralogy whereas a comparatively higher value (Avg. > 0.42) in the Rampur shale may be due to diagenetic K_2O enrichment (Fig. 2b) (Cox et al., 1995). Further, variation of SiO_2/Al_2O_3 in a narrow range and near horizontal plotting of samples in SiO_2/Al_2O_3 *vs.* K_2O/Na_2O crossplot suggest their derivation dominantly from recycled felsic source (Ohta, 2004).

4.2. Trace element geochemistry

Trace element concentrations of lower and upper Vindhyan shales are provided in Table 2. On comparison with Post-Archean Australian Shale (PAAS), Vindhyan shales show depletion in Sc, Co, Ni, Cu, Zn, Sr, Ba, Zr, Nb and enrichment in Pb and U. A wide variation is noticed in concentrations of Cr, V, Rb, Y, Hf and Th (Taylor and McLennan, 1985) (Fig. 3). The Vindhyan shales are low in large ion lithophile elements (LILE: Rb, Sr, Ba) and transition trace element (TTE: Sc, Co, Cr, Ni, V, Cu) except for the Rewa and Bijaygarh shales. In the Rewa shale, Rb and Ba values are relatively enriched among LILE because of higher detrital flux of feldspar (Fig. 3).

The trace elements like TiO_2, Rb, Sr, Ba and Th in fine-grained sedimentary rocks are immobile in a natural sedimentary environment and transported as detrital flux in sedimentary basin (Hayashi et al., 1997; Hu et al., 2020). Concentration of these elements in Vindhyan shales are compared with Al_2O_3. In Arangi shale, Rb and Ba are positively correlated with Al_2O_3 (linear correlation coefficient, r = 0.98, 0.95) indicating that these elements are fixed in K-rich clays (illites) and K-feldspars whereas Sc, Th, and Sr are negatively correlated (r = −0.87, −0.78 and −0.77) suggesting effect of chemical alteration and hydraulic sorting. High field strength elements (HFSEs) like Zr, Nb and Ti are positively correlated with Al_2O_3 in the Arangi shale (r = 0.80, 0.66 and 0.97) and are likely to

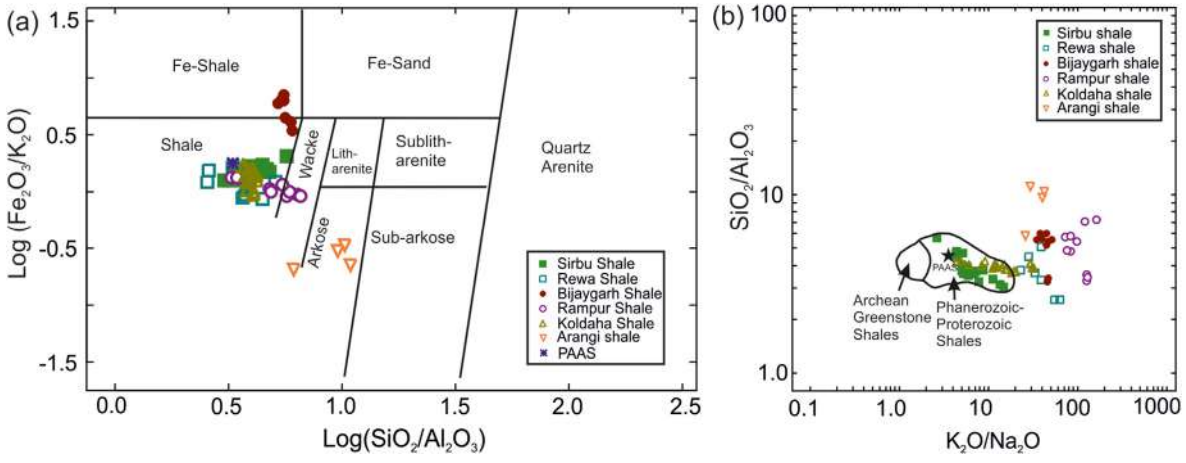

Fig. 2. (a) Geochemical classification diagram using Log (SiO_2/Al_2O_3)- Log (Fe_2O_3/K_2O) for Vindhyan shale samples (modified after Herron, 1988). Note: Plotting of Arangi shale in "Arkose field", almost mimicking its source composition; (b) SiO_2/Al_2O_3–K_2O/Na_2O crossplot showing distribution of Vindhyan shale samples in the Phanerozoic-Proterozoic shales field and their comparison with PAAS standard data (after Taylor and McLennan, 1985). Note: The higher K_2O/Na_2O ratio in Vindhyan shales in comparison to the Phanerozoic/Proterozoic shales indicates clay mineral dominance and K-metasomatism in sediment composition.

Table 2
Trace and rare earth element concentrations (ppm) along with elemental ratios of Vindhyan shales.

Shale samples	N1/28	N2/28	N3/28	N4/28	N5/28	N6/28	N7/28	N8/28	N9/28	N10/28	SS1	SS2	SS3	SS4
Sirbu shale														
Sc	11.0	9.0	6.2	9.0	8.2	15.7	9.9	12.5	9.2	9.6	6.9	9.9	13.9	10.0
V	101.0	94.0	66.0	86.0	78.0	121.0	81.0	98.0	89.0	81.0	69.0	90.0	112.0	94.0
Cr	146.0	109.0	105.0	88.0	82.0	112.0	80.0	80.0	101.0	95.0	131.0	78.0	86.0	93.0
Co	13.0	13.0	12.0	11.0	9.0	17.0	3.0	10.0	12.0	12.0	8.0	13.0	12.0	8.0
Ni	32.0	28.0	27.0	29.0	27.0	38.0	20.0	26.0	32.0	28.0	27.0	30.0	32.0	27.0
Cu	31.0	25.0	23.0	24.0	25.0	30.0	21.0	30.0	28.0	33.0	28.0	21.0	24.0	30.0
Zn	69.0	66.0	73.0	66.0	55.0	122.0	71.0	79.0	100.0	61.0	39.0	76.0	84.0	85.0
Ga	18.0	18.0	13.0	16.0	14.0	22.0	16.0	18.0	18.0	17.0	13.0	18.0	22.0	19.0
Rb	170.0	146.0	90.0	131.0	128.0	228.0	131.0	165.0	151.0	133.0	109.0	151.0	213.0	153.0
Sr	93.0	80.0	50.0	67.0	52.0	132.0	74.0	80.0	71.0	70.0	63.0	84.0	105.0	87.0
Y	30.0	34.0	32.0	30.0	27.0	46.0	27.0	36.0	29.0	29.0	26.0	29.0	29.0	30.0
Zr	230.0	301.0	324.0	249.0	190.0	197.0	285.0	203.0	215.0	199.0	227.0	210.0	208.0	218.0
Nb	17.0	17.0	14.0	15.0	11.0	14.0	14.0	15.0	14.0	13.0	12.0	14.0	16.0	15.0
Cs	11.1	9.0	5.3	8.0	8.2	15.6	7.3	9.0	9.8	8.1	8.2	9.3	12.3	9.3
Ba	466.0	478.0	402.0	469.0	360.0	598.0	413.0	518.0	461.0	488.0	333.0	438.0	542.0	444.0
La	49.6	47.8	31.5	40.8	29.4	49.9	46.5	39.1	43.4	33.5	28.0	43.3	50.2	45.7
Ce	95.9	94.0	66.7	79.4	57.8	117.0	88.1	77.8	89.7	69.7	57.5	84.0	97.2	87.9
Pr	9.9	9.9	6.7	8.3	6.3	13.8	9.2	8.1	10.2	7.6	6.4	9.0	10.5	9.2
Nd	41.4	42.1	26.5	34.0	26.9	66.9	38.1	33.7	46.4	32.0	25.3	36.0	41.1	36.1
Sm	7.0	7.1	5.7	6.1	5.0	20.5	6.9	5.8	11.0	6.3	5.3	6.8	6.8	6.1
Eu	1.3	1.3	1.2	1.2	1.0	4.1	1.2	1.1	2.2	1.2	1.0	1.3	1.2	1.1
Gd	5.1	5.4	4.8	4.7	3.9	15.6	5.0	4.4	8.7	4.7	3.9	5.1	4.8	4.7
Tb	1.0	1.1	1.0	1.0	0.8	2.7	1.0	0.9	1.6	0.9	0.8	1.0	0.9	0.9
Dy	5.5	6.2	5.5	5.6	4.6	12.5	5.3	5.1	8.3	5.0	4.3	5.3	5.3	5.4
Ho	1.2	1.3	1.2	1.2	1.0	2.1	1.1	1.0	1.6	1.0	0.9	1.1	1.1	1.2
Er	3.4	3.8	3.2	3.5	2.8	5.5	3.3	3.2	4.3	3.0	2.6	3.1	3.4	3.4
Tm	0.5	0.6	0.5	0.6	0.5	0.8	0.5	0.5	0.6	0.5	0.4	0.5	0.5	0.6
Yb	3.0	3.4	3.0	3.1	2.5	4.0	2.9	2.8	3.4	2.6	2.3	2.7	3.0	3.1
Lu	0.5	0.5	0.5	0.5	0.4	0.6	0.5	0.4	0.5	0.4	0.4	0.4	0.5	0.5
Hf	8.6	10.4	10.1	8.7	6.8	8.5	9.7	7.8	7.3	7.2	7.7	8.1	8.9	7.1
Ta	1.5	1.4	1.1	1.2	1.1	1.6	1.2	1.2	1.3	1.0	1.3	1.3	1.2	1.6
Pb	32.0	30.0	31.0	28.0	28.0	43.0	32.0	29.0	31.0	29.0	28.0	30.0	32.0	34.0
Th	21.0	22.0	18.0	19.0	15.0	23.0	18.0	20.0	18.0	16.0	15.0	19.0	22.0	21.0
U	2.3	2.7	4.6	2.0	2.5	5.6	2.6	4.1	2.3	3.6	1.7	2.6	3.8	2.5
Th/Sc	1.9	2.4	2.9	2.1	1.8	1.5	1.8	1.6	2.0	1.7	2.2	1.9	1.6	2.1
Th/Co	1.6	1.7	1.5	1.7	1.7	1.4	6.0	2.0	1.5	1.3	1.9	1.5	1.8	2.6
Th/Cr	0.1	0.2	0.2	0.2	0.2	0.2	0.2	0.3	0.2	0.2	0.1	0.2	0.3	0.2
Cr/Th	7.0	5.0	5.8	4.6	5.5	4.9	4.4	4.0	5.6	5.9	8.7	4.1	3.9	4.4
La/Sc	4.5	5.3	5.1	4.5	3.6	3.2	4.7	3.1	4.7	3.5	4.1	4.4	3.6	4.6
Cr/Ni	4.6	3.9	3.9	3.0	3.0	2.9	4.0	3.1	3.2	3.4	4.9	2.6	2.7	3.4
$(Gd/Yb)_{CN}$	1.4	1.3	1.3	1.2	1.3	3.2	1.4	1.3	2.1	1.5	1.4	1.5	1.3	1.2
Eu/Eu*	0.7	0.6	0.7	0.7	0.7	0.7	0.6	0.7	0.7	0.7	0.7	0.7	0.6	0.6
ΣL/ΣH	10.2	9.1	7.1	8.5	7.8	6.2	9.8	9.1	7.0	8.3	7.9	9.5	10.6	9.5
∑REE	225.1	224.2	157.8	189.7	142.6	315.9	209.4	183.9	231.9	168.4	139.1	199.4	226.5	205.8

Shale samples	SS5	SBS3	SBS4	SBS5	SBS6	SBS7	SBS8	SBS9	SBS10	PS1	PS2	PS3	PS4	PS5
Sirbu shale										Rewa shale				
Sc	12.6	10.9	10.7	11.1	11.8	11.3	9.9	14.8	10.4	12.6	12.3	20.8	19.2	16.9
V	107.0	103.0	100.0	90.0	106.0	107.0	93.0	111.0	88.0	59.2	70.5	104.4	166.7	124.9
Cr	97.0	83.0	101.0	139.0	124.0	84.0	91.0	99.0	159.0	113.3	109.4	112.7	112.5	111.8
Co	13.0	7.0	7.0	15.0	17.0	12.0	9.0	17.0	12.0	6.1	5.3	3.8	3.7	12.0
Ni	32.0	27.0	26.0	28.0	29.0	28.0	29.0	34.0	28.0	19.0	22.6	119.7	47.8	37.3
Cu	29.0	26.0	27.0	24.0	30.0	28.0	26.0	34.0	30.0	24.6	26.6	33.5	82.2	67.9
Zn	92.0	70.0	79.0	64.0	73.0	63.0	64.0	177.0	105.0	88.3	39.5	722.5	286.5	69.0
Ga	20.0	21.0	18.0	18.0	19.0	22.0	16.0	21.0	15.0	18.8	15.5	22.1	22.1	28.5
Rb	187.0	176.0	165.0	155.0	190.0	198.0	165.0	204.0	148.0	207.7	131.8	209.9	205.8	252.0
Sr	91.0	87.0	73.0	65.0	80.0	85.0	67.0	86.0	59.0	115.4	34.2	109.5	91.6	110.1
Y	32.0	29.0	30.0	28.0	32.0	27.0	29.0	31.0	29.0	37.4	51.4	179.1	98.7	49.4
Zr	199.0	185.0	227.0	229.0	209.0	187.0	205.0	217.0	229.0	160.2	170.4	250.1	233.5	243.2
Nb	16.0	15.0	13.0	13.0	14.0	15.0	14.0	13.0	14.0	16.2	10.8	17.1	17.7	23.5
Cs	10.5	9.2	9.5	9.9	8.1	8.3	13.4	8.2	9.7	13.6	10.2	19.2	16.6	17.4
Ba	478.0	502.0	458.0	526.0	465.0	522.0	475.0	502.0	461.0	612.2	353.8	664.8	1246.9	1172.8
La	50.1	45.4	45.2	43.8	45.2	53.1	48.2	44.7	39.1	68.7	31.4	65.9	77.9	71.3
Ce	95.9	88.4	86.6	82.2	88.1	102.0	89.0	83.6	75.7	128.4	59.2	138.8	163.4	143.3
Pr	10.5	9.4	9.2	8.6	9.7	10.3	9.7	9.0	8.2	13.2	8.2	17.4	18.6	16.0
Nd	40.5	38.7	36.3	34.7	41.7	41.3	38.9	39.4	34.2	46.6	34.1	76.2	74.7	59.3
Sm	8.3	6.6	6.9	6.1	7.9	6.3	5.8	7.6	6.2	8.2	7.2	18.3	14.5	9.9
Eu	1.6	1.2	1.2	1.2	1.5	1.2	1.2	1.4	1.1	1.4	1.4	3.9	2.9	1.8
Gd	6.2	4.8	4.9	4.6	5.9	4.8	4.6	5.6	4.7	7.3	7.1	22.1	13.8	8.6
Tb	1.2	0.9	0.9	0.9	1.1	0.9	1.0	1.1	1.0	1.2	1.3	4.4	2.4	1.4
Dy	6.5	5.2	5.1	4.9	6.3	5.2	5.6	6.0	5.4	6.8	7.5	27.5	15.1	8.5
Ho	1.3	1.1	1.1	1.0	1.3	1.1	1.2	1.2	1.1	1.5	1.7	6.2	3.6	1.9
Er	3.8	3.2	3.2	3.0	3.7	3.3	3.4	3.6	3.3	3.8	4.3	14.9	9.8	5.3

Table 2 (*continued*)

Shale samples	SS5	SBS3	SBS4	SBS5	SBS6	SBS7	SBS8	SBS9	SBS10	PS1	PS2	PS3	PS4	PS5
Sirbu shale										Rewa shale				
Tm	0.6	0.5	0.5	0.5	0.6	0.6	0.6	0.6	0.5	0.6	0.6	2.1	1.5	0.8
Yb	3.3	2.8	2.7	2.7	3.1	3.0	3.1	3.2	2.9	4.1	4.1	13.4	11.0	5.6
Lu	0.5	0.4	0.4	0.4	0.5	0.5	0.5	0.5	0.5	0.6	0.6	2.0	1.7	0.8
Hf	9.3	7.5	7.6	7.6	8.7	8.2	8.0	6.5	7.5	5.0	5.0	7.5	6.7	7.8
Ta	1.8	1.2	1.3	1.9	1.1	1.5	1.5	1.7	1.6	1.5	0.9	1.6	1.7	2.3
Pb	30.0	27.0	36.0	35.0	35.0	35.0	29.0	35.0	33.0	25.8	14.1	100.4	218.1	26.5
Th	21.0	19.0	21.0	19.0	22.0	21.0	19.0	21.0	20.0	34.8	11.8	27.2	30.1	39.8
U	4.4	2.7	1.3	4.1	3.7	1.4	2.8	4.5	2.8	2.9	1.8	4.7	7.8	6.2
Th/Sc	1.7	1.7	2.0	1.7	1.9	1.9	1.9	1.4	1.9	2.8	1.0	1.3	1.6	2.4
Th/Co	1.6	2.7	3.0	1.3	1.3	1.8	2.1	1.2	1.7	5.7	2.2	7.1	8.0	3.3
Th/Cr	0.2	0.2	0.2	0.1	0.2	0.3	0.2	0.2	0.1	0.3	0.1	0.2	0.3	0.4
Cr/Th	4.6	4.4	4.8	7.3	5.6	4.0	4.8	4.7	8.0	3.3	9.3	4.1	3.7	2.8
La/Sc	4.0	4.2	4.2	3.9	3.8	4.7	4.9	3.0	3.8	5.5	2.5	3.2	4.0	4.2
Cr/Ni	3.0	3.1	3.9	5.0	4.3	3.0	3.1	2.9	5.7	6.0	4.8	0.9	2.4	3.0
$(Gd/Yb)_{CN}$	1.5	1.4	1.5	1.4	1.5	1.3	1.2	1.4	1.3	1.5	1.4	1.3	1.0	1.2
Eu/Eu*	0.7	0.7	0.7	0.7	0.7	0.6	0.7	0.7	0.6	0.6	0.6	0.6	0.6	0.6
ΣL/ΣH	8.9	10.0	9.8	9.8	8.6	11.1	9.8	8.5	8.5	10.3	5.2	3.5	6.0	9.1
∑REE	230.1	208.7	204.3	194.6	216.7	233.5	212.5	207.5	183.9	292.4	168.6	413.1	410.9	334.6

Shale samples	PS6	JS1	BGS1	BGS2	BGS3	BGS4	BGS5	BGS6	BGS7	RN1	RN2	RN3	RN4	BS1
Rewa shale			Bijaygarh shale							Rampur shale				
Sc	20.1	20.1	15.0	13.0	12.0	16.0	14.0	12.0	11.0	12.0	8.7	9.7	8.5	20.1
V	132.9	159.4	259.0	255.0	226.0	260.0	245.0	240.0	230.0	114.5	142.2	197.4	181.1	140.0
Cr	113.5	113.1	106.0	89.0	85.0	102.0	84.0	79.0	70.0	116.5	117.6	118.5	115.9	114.0
Co	9.3	14.9	43.0	76.0	64.0	44.0	45.0	65.0	49.0	6.9	4.6	6.1	6.1	3.0
Ni	28.2	35.9	76.0	142.0	106.0	71.0	98.0	86.0	96.0	36.5	31.7	52.9	43.2	26.0
Cu	17.6	20.9	48.0	95.0	85.0	45.0	75.0	74.0	66.0	40.9	25.6	55.8	44.2	3.0
Zn	79.6	76.7	70.0	101.0	86.0	68.0	81.0	74.0	68.0	65.9	49.4	240.4	92.1	10.0
Ga	32.5	25.7	14.0	14.0	13.0	14.0	13.0	14.0	14.0	17.3	9.8	15.2	16.3	8.0
Rb	276.7	246.8	153.0	159.0	157.0	163.0	155.0	161.0	151.0	201.1	108.6	155.5	173.1	53.0
Sr	136.1	146.2	107.0	69.0	130.0	105.0	124.0	136.0	142.0	31.6	37.9	70.9	44.2	24.0
Y	71.3	44.2	56.0	67.0	67.0	58.0	63.0	61.0	62.0	39.9	23.6	21.7	21.1	16.0
Zr	221.7	244.7	171.0	174.0	174.0	172.0	177.0	172.0	178.0	204.8	103.3	133.4	148.1	40.0
Nb	22.2	17.7	12.0	10.0	11.0	12.0	13.0	12.0	12.0	11.6	7.0	9.5	9.9	5.0
Cs	20.5	18.5	15.0	14.0	19.0	13.0	14.0	15.0	12.0	10.9	4.1	6.0	6.7	5.7
Ba	853.9	435.7	357.0	316.0	346.0	363.0	365.0	354.0	334.0	409.5	217.8	407.9	411.5	438.0
La	94.3	59.8	45.0	46.0	48.0	44.0	42.0	43.0	41.0	40.9	24.8	26.1	27.2	31.0
Ce	192.8	122.9	91.0	91.0	100.0	91.0	90.0	95.0	100.0	79.5	49.5	51.9	50.9	52.8
Pr	21.7	13.9	9.4	9.2	9.8	9.4	9.2	9.2	9.6	9.9	5.8	6.1	6.6	6.1
Nd	80.6	52.8	39.9	41.2	43.1	41.2	41.2	41.1	42.0	38.4	22.3	23.4	24.9	24.1
Sm	13.9	9.2	7.8	8.7	8.9	8.4	8.4	8.2	8.4	7.1	4.1	4.3	4.4	4.7
Eu	2.3	1.7	1.7	1.8	1.9	1.7	1.8	1.7	1.8	1.3	0.8	0.8	0.8	0.9
Gd	12.0	8.3	6.5	7.3	7.6	6.9	7.0	6.9	7.1	6.5	3.8	3.8	3.9	3.7
Tb	2.0	1.4	1.4	1.5	1.5	1.5	1.5	1.5	1.4	1.1	0.6	0.6	0.6	0.7
Dy	11.8	7.7	8.0	9.2	9.3	9.0	8.9	8.7	8.2	6.2	3.6	3.4	3.1	4.0
Ho	2.7	1.7	1.7	2.0	2.0	2.0	1.9	1.9	1.7	1.4	0.8	0.8	0.7	0.8
Er	7.2	4.5	5.1	5.9	5.5	5.6	5.6	5.6	5.1	3.6	2.1	2.0	1.8	2.3
Tm	1.1	0.7	0.8	0.9	0.9	0.9	0.9	0.9	0.8	0.5	0.3	0.3	0.3	0.4
Yb	7.1	4.3	4.5	4.9	4.7	4.9	4.8	4.7	4.5	3.4	2.1	2.0	1.8	1.9
Lu	1.0	0.7	0.7	0.8	0.7	0.7	0.7	0.7	0.7	0.5	0.3	0.3	0.3	0.3
Hf	7.1	7.5	2.2	2.0	1.9	2.3	2.1	2.0	2.4	6.1	3.2	4.0	4.3	5.3
Ta	2.0	1.7	1.1	1.2	1.2	1.0	1.5	1.6	1.9	1.1	0.7	0.8	0.9	1.1
Pb	28.2	19.6	28.0	22.0	58.0	33.0	28.0	34.0	7.0	30.7	19.5	33.9	30.6	39.0
Th	44.6	24.7	24.0	14.0	18.0	17.0	19.0	20.0	21.0	20.0	11.3	10.8	12.1	5.0
U	4.5	3.3	27.0	31.0	26.0	26.0	24.1	26.5	26.0	7.0	7.1	10.0	8.8	1.5
Th/Sc	2.2	1.2	1.6	1.1	1.5	1.1	1.4	1.7	1.9	1.7	1.3	1.1	1.4	0.2
Th/Co	4.8	1.7	0.6	0.2	0.3	0.4	0.4	0.3	0.4	2.9	2.5	1.8	2.0	1.7
Th/Cr	0.4	0.2	0.2	0.2	0.2	0.2	0.2	0.3	0.3	0.2	0.1	0.1	0.1	0.0
Cr/Th	2.5	4.6	4.4	6.4	4.7	6.0	4.4	4.0	3.3	5.8	10.4	11.0	9.6	22.8
La/Sc	4.7	3.0	3.0	3.5	4.0	2.8	3.0	3.6	3.7	3.4	2.8	2.7	3.2	1.5
Cr/Ni	4.0	3.2	1.4	0.6	0.8	1.4	0.9	0.9	0.7	3.2	3.7	2.2	2.7	4.4
$(Gd/Yb)_{CN}$	1.4	1.5	1.2	1.2	1.3	1.2	1.2	1.2	1.3	1.5	1.5	1.6	1.8	1.5
Eu/Eu*	0.6	0.6	0.7	0.7	0.7	0.7	0.7	0.7	0.7	0.6	0.6	0.6	0.6	0.7
ΣL/ΣH	9.1	8.9	6.8	6.1	6.6	6.2	6.1	6.4	6.9	7.6	7.8	8.6	9.3	8.5
∑REE	450.5	289.5	223.5	230.3	243.7	227.2	224.0	229.0	232.3	200.4	121.0	125.7	127.2	133.6

Shale samples	BS2	BS3	RS1	RS2	RS3	KSK1	KSK2	KSK3	KSK4	KSK5	KS1	KS2	KS3	KS4	GS1
Rampur shale						Koldaha shale									
Sc	4.4	9.6	6.4	10.5	7.3	15.0	16.4	17.3	16.8	13.2	8.7	9.2	7.8	10.0	10.3
V	123.0	153.0	141.0	140.1	151.1	108.9	104.1	118.4	106.0	81.9	96.0	112.0	106.0	104.2	97.0
Cr	112.0	117.0	116.0	112.0	110.0	116.7	114.0	114.7	114.0	114.4	110.2	112.3	114.5	115.6	84.0
Co	4.0	6.0	28.0	10.0	14.0	14.8	11.5	14.6	12.3	15.7	10.0	11.0	7.0	7.0	13.0

(*continued on next page*)

Table 2 (*continued*)

Shale samples	BS2	BS3	RS1	RS2	RS3	KSK1	KSK2	KSK3	KSK4	KSK5	KS1	KS2	KS3	KS4	GS1
Rampur shale						Koldaha shale									
Ni	56.0	47.0	26.0	26.0	25.0	35.8	27.7	29.4	27.0	23.7	26.0	35.0	34.0	29.0	24.0
Cu	30.0	11.0	22.0	3.0	62.0	37.7	34.6	20.8	39.7	15.4	3.0	61.0	61.0	17.0	11.0
Zn	19.0	12.0	32.0	26.0	38.0	143.0	92.2	78.5	83.2	67.2	50.0	124.0	88.0	79.0	73.0
Ga	15.0	14.0	18.0	20.0	19.0	20.3	21.2	22.9	22.1	17.8	17.0	16.0	15.0	17.0	17.0
Rb	170.0	130.0	234.0	262.0	234.0	191.1	205.6	227.6	211.8	181.8	225.0	164.0	163.0	178.0	199.0
Sr	27.0	27.0	22.0	21.0	23.0	65.3	34.1	34.2	39.0	42.8	34.0	47.0	39.0	40.0	39.0
Y	23.0	23.0	28.0	26.0	28.0	42.5	40.5	36.6	41.0	35.5	25.0	29.0	29.0	31.0	30.0
Zr	117.0	107.0	166.0	163.0	174.0	232.3	249.1	223.1	247.3	272.4	143.0	226.0	223.0	271.0	212.0
Nb	10.0	10.0	11.0	12.0	12.0	10.7	11.5	11.7	12.1	11.8	8.0	11.0	12.0	12.0	12.0
Cs	8.1	6.5	6.0	6.5	7.8	15.6	17.5	21.0	19.2	14.9	14.8	18.6	16.7	18.5	13.4
Ba	445.0	413.0	410.0	421.0	446.0	385.2	398.2	331.3	421.6	753.0	651.0	384.0	441.0	456.0	439.0
La	43.4	60.0	57.2	54.8	57.0	42.7	45.2	43.9	45.1	40.9	40.8	48.7	46.7	51.0	49.1
Ce	71.7	114.5	103.0	96.4	109.2	87.9	93.1	87.0	91.9	85.3	77.9	90.7	87.6	95.1	95.2
Pr	8.7	12.6	12.2	9.9	12.3	10.0	10.6	10.0	10.5	9.8	8.3	9.9	9.5	10.3	10.4
Nd	34.6	50.6	50.5	39.0	49.7	39.3	41.6	37.6	41.0	38.1	34.6	41.2	37.8	42.6	42.5
Sm	6.1	8.6	9.1	6.8	9.0	7.7	7.9	6.7	7.7	7.0	6.4	7.8	7.0	8.0	7.7
Eu	1.1	1.5	1.6	1.2	1.7	1.6	1.6	1.3	1.5	1.5	1.3	1.5	1.3	1.5	1.5
Gd	4.6	6.3	6.7	5.3	6.6	7.2	7.0	5.9	6.8	6.4	4.8	6.0	5.4	5.9	5.6
Tb	0.8	1.1	1.2	1.0	1.2	1.2	1.2	1.0	1.1	1.0	0.9	1.1	1.0	1.1	1.0
Dy	4.3	6.0	6.5	5.7	6.4	7.3	6.8	6.0	6.9	5.9	5.1	6.3	5.7	6.2	5.5
Ho	0.9	1.2	1.3	1.2	1.3	1.6	1.6	1.4	1.5	1.4	1.1	1.3	1.2	1.3	1.1
Er	2.6	3.5	3.8	3.5	3.8	4.0	3.9	3.7	4.0	3.5	3.2	3.9	3.6	3.8	3.3
Tm	0.4	0.5	0.6	0.6	0.6	0.6	0.6	0.5	0.6	0.5	0.5	0.6	0.6	0.6	0.9
Yb	2.1	3.0	3.2	3.0	3.3	4.0	3.9	3.7	4.1	3.7	2.8	3.5	3.2	3.4	2.9
Lu	0.3	0.4	0.5	0.5	0.5	0.6	0.6	0.6	0.6	0.6	0.4	0.5	0.5	0.5	0.5
Hf	5.0	4.4	3.9	5.2	4.6	6.9	7.4	6.8	7.4	8.0	7.5	7.0	7.9	7.9	7.5
Ta	0.9	0.9	1.0	0.8	1.3	0.9	1.0	1.1	0.9	1.1	1.0	1.0	1.2	1.0	1.0
Pb	36.0	74.0	21.0	20.0	19.0	30.4	21.1	17.0	18.6	16.9	19.0	47.0	45.0	38.0	27.0
Th	16.0	16.0	18.0	18.0	18.0	13.1	19.8	19.8	20.4	19.7	14.0	17.0	17.0	18.0	18.0
U	12.3	5.8	1.0	1.0	1.6	4.3	3.6	3.6	3.8	3.8	1.0	2.1	3.9	5.3	3.2
Th/Sc	3.6	1.7	2.8	1.7	2.5	0.9	1.2	1.1	1.2	1.5	1.6	1.8	2.2	1.8	1.7
Th/Co	4.0	2.7	0.6	1.8	1.3	0.9	1.7	1.4	1.7	1.3	1.4	1.5	2.4	2.6	1.4
Th/Cr	0.1	0.1	0.2	0.2	0.2	0.1	0.2	0.2	0.2	0.2	0.1	0.2	0.1	0.2	0.2
Cr/Th	7.0	7.3	6.4	6.2	6.1	8.9	5.8	5.8	5.6	5.8	7.9	6.6	6.7	6.4	4.7
La/Sc	9.9	6.3	8.9	5.2	7.8	2.8	2.8	2.5	2.7	3.1	4.7	5.3	6.0	5.1	4.8
Cr/Ni	2.0	2.5	4.5	4.3	4.4	3.3	4.1	3.9	4.2	4.8	4.2	3.2	3.4	4.0	3.5
$(Gd/Yb)_{CN}$	1.8	1.7	1.7	1.4	1.6	1.5	1.5	1.3	1.4	1.4	1.4	1.4	1.4	1.4	1.6
Eu/Eu*	0.6	0.6	0.6	0.6	0.7	0.7	0.6	0.6	0.7	0.7	0.7	0.7	0.7	0.7	0.7
ΣL/ΣH	10.4	11.3	9.8	10.0	10.0	7.2	7.9	8.2	7.7	8.0	9.0	8.5	9.0	9.2	9.9
∑REE	181.6	269.8	257.4	228.9	262.7	215.8	225.5	209.4	223.3	205.6	188.0	223.1	211.0	231.2	227.2

Shale samples	GS2	GS3	GS4	GS5	GS6	GS7	GS8	KDS0	KDS1	KDS2	KDS3	B31	B32	B34	B35
Koldaha shale												Arangi shale			
Sc	11.2	10.9	9.6	9.7	8.7	9.3	9.7	9.5	11.2	10.0	9.1	6.5	2.4	5.1	4.2
V	91.0	91.0	89.0	84.0	89.0	91.0	93.0	86.0	93.0	81.0	74.0	369.0	133.0	264.0	229.0
Cr	58.0	56.0	54.0	56.0	67.0	57.0	74.0	86.0	85.0	104.0	103.0	61.0	70.0	85.0	79.0
Co	10.0	13.0	16.0	15.0	18.0	14.0	10.0	20.0	10.0	11.0	10.0	3.0	7.0	7.0	4.0
Ni	26.0	26.0	26.0	26.0	25.0	23.0	26.0	39.0	33.0	32.0	31.0	9.0	16.0	19.0	15.0
Cu	28.0	12.0	8.0	29.0	3.0	16.0	14.0	33.0	48.0	35.0	21.0	17.0	6.0	11.0	8.0
Zn	59.0	57.0	59.0	54.0	49.0	46.0	88.0	40.0	39.0	31.0	23.0	8.0	2.0	2.0	2.0
Ga	18.0	20.0	20.0	18.0	19.0	19.0	20.0	20.0	19.0	16.0	16.0	10.0	14.0	12.0	12.0
Rb	216.0	233.0	228.0	222.0	225.0	243.0	219.0	221.0	227.0	198.0	186.0	44.0	166.0	58.0	55.0
Sr	39.0	39.0	37.0	38.0	35.0	35.0	37.0	31.0	35.0	38.0	38.0	35.0	21.0	37.0	52.0
Y	29.0	30.0	29.0	30.0	29.0	28.0	29.0	32.0	30.0	28.0	28.0	13.0	14.0	15.0	15.0
Zr	158.0	162.0	163.0	163.0	160.0	169.0	174.0	157.0	163.0	187.0	193.0	95.0	119.0	115.0	105.0
Nb	11.0	10.0	10.0	11.0	11.0	11.0	11.0	11.0	10.0	11.0	10.0	9.0	10.0	9.0	7.0
Cs	15.7	17.7	15.4	16.4	17.2	18.5	18.7	16.3	12.0	13.2	14.6	15.7	17.7	15.4	16.4
Ba	535.0	575.0	433.0	391.0	522.0	419.0	373.0	392.0	587.0	596.0	827.0	146.0	464.0	198.0	257.0
La	50.7	53.0	53.7	53.3	50.2	56.4	49.8	52.7	53.3	48.6	46.3	26.8	13.9	32.5	30.5
Ce	94.9	99.0	99.6	100.6	94.5	103.5	92.5	100.9	101.6	93.6	90.5	49.3	18.7	58.8	57.0
Pr	10.2	10.7	10.4	10.8	10.2	10.8	10.0	10.7	11.3	10.4	9.9	5.3	1.3	6.2	6.1
Nd	41.9	43.8	42.2	43.9	42.0	43.3	40.9	44.0	47.4	43.3	41.2	20.6	3.9	23.7	23.5
Sm	7.1	7.4	7.1	7.3	7.2	7.2	6.9	8.1	8.3	7.8	7.8	3.7	0.6	3.9	4.5
Eu	1.5	1.5	1.4	1.4	1.4	1.4	1.4	1.5	1.6	1.5	1.6	0.7	0.3	0.7	0.9
Gd	5.3	5.4	5.4	5.3	5.3	5.4	5.2	6.1	6.0	5.5	5.6	2.7	0.7	3.5	4.4
Tb	1.0	1.0	1.0	1.0	1.0	1.0	1.0	1.2	1.1	1.0	1.1	0.4	0.1	0.6	0.8
Dy	5.2	5.5	5.5	5.3	5.2	5.5	5.3	6.5	6.3	5.8	6.0	2.4	1.0	3.1	3.9
Ho	1.1	1.1	1.2	1.1	1.1	1.2	1.1	1.3	1.3	1.2	1.2	0.5	0.3	0.6	0.7
Er	3.2	3.3	3.4	3.3	3.2	3.4	3.2	3.9	3.6	3.5	3.6	1.5	0.9	1.8	1.9
Tm	0.8	0.5	0.5	0.5	0.5	0.5	0.5	0.6	0.6	0.5	0.6	0.2	0.2	0.3	0.3
Yb	2.8	2.9	3.0	2.8	2.8	2.9	2.8	3.3	3.2	3.0	3.1	1.4	1.1	1.7	1.6
Lu	0.4	0.5	0.5	0.4	0.4	0.5	0.4	0.5	0.5	0.5	0.5	0.2	0.2	0.3	0.3
Hf	7.5	7.3	7.4	7.7	7.1	7.0	7.6	8.0	7.8	7.8	7.4	8.0	7.9	7.7	7.2

Table 2 (*continued*)

Shale samples	GS2	GS3	GS4	GS5	GS6	GS7	GS8	KDS0	KDS1	KDS2	KDS3	B31	B32	B34	B35
Koldaha shale												Arangi shale			
Ta	1.1	1.2	1.0	1.1	1.1	1.1	1.4	1.1	1.0	1.1	1.2	1.0	1.1	1.2	1.0
Pb	20.0	23.0	21.0	19.0	20.0	20.0	21.0	19.0	25.0	23.0	24.0	25.0	20.0	24.0	33.0
Th	17.0	18.0	18.0	17.0	18.0	18.0	18.0	17.0	17.0	15.0	16.0	9.0	5.0	12.0	10.0
U	2.2	1.5	3.3	4.0	1.0	1.0	1.7	1.2	2.2	2.3	2.1	7.1	0.9	6.9	8.1
Th/Sc	1.5	1.7	1.9	1.8	2.1	1.9	1.9	1.8	1.5	1.5	1.8	1.4	2.1	2.4	2.4
Th/Co	1.7	1.4	1.1	1.1	1.0	1.3	1.8	0.9	1.7	1.4	1.6	3.0	0.7	1.7	2.5
Th/Cr	0.3	0.3	0.3	0.3	0.3	0.3	0.2	0.2	0.2	0.1	0.2	0.1	0.1	0.1	0.1
Cr/Th	3.4	3.1	3.0	3.3	3.7	3.2	4.1	5.1	5.0	6.9	6.4	6.8	14.0	7.1	7.9
La/Sc	4.5	4.9	5.6	5.5	5.8	6.1	5.1	5.5	4.8	4.9	5.1	4.1	5.8	6.4	7.3
Cr/Ni	2.2	2.2	2.1	2.2	2.7	2.5	2.8	2.2	2.6	3.3	3.3	6.8	4.4	4.5	5.3
$(Gd/Yb)_{CN}$	1.5	1.5	1.5	1.5	1.5	1.5	1.5	1.5	1.5	1.5	1.5	5.3	5.8	5.7	5.2
Eu/Eu*	0.7	0.7	0.7	0.7	0.7	0.7	0.7	0.7	0.7	0.7	0.7	0.8	0.2	0.7	0.8
ΣL/ΣH	10.4	10.6	10.5	11.0	10.6	10.9	10.3	9.4	9.9	9.7	9.1	11.5	8.8	10.6	8.9
∑REE	226.1	235.6	234.9	237.1	224.9	243.0	220.9	241.2	246.1	226.2	218.9	115.6	126.7	137.8	135.1

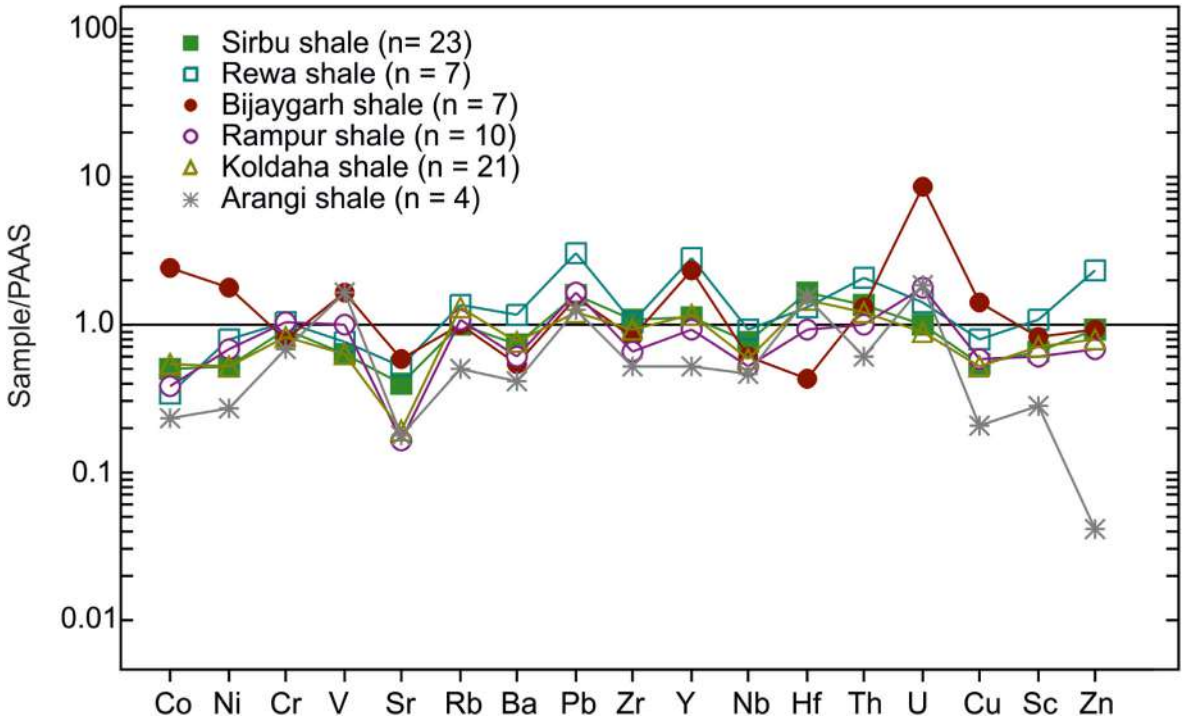

Fig. 3. PAAS normalized trace element distribution of Vindhyan shale samples. The PAAS values are taken from Taylor and McLennan (1985).

be bound in clay minerals. The concentration of Rb, Sr, Ba and Th are moderately correlated with Al_2O_3 in the Koldaha shale (r = 0.60, 0.61, 0.25 and 0.74), moderately to strongly correlated in the Rampur shale (r = 0.96, 0.41, 0.44 and 0.82), the Rewa shale (r = 0.90, 0.64, 0.65 and 0.83) and the Sirbu shale (r = 0.92, 0.81, 0.71 and 0.75) suggesting fixation of these elements in K-feldspar and clay minerals. Very low to low correlation values for these elements with Al_2O_3 (r = 0.37, 0.30, 0.49 and 0.10) are recorded only from the Bijaygarh shale. Similarly, concentrations of Al_2O_3 is negatively or poorly correlated with HFSEs like Zr, Nb and Ti in the Koldaha shale (0.10, 0.17 and 0.10), the Bijaygarh shale (−0.14, 0.54 and 0.10) and the Sirbu shale (−0.47, 0.35, 0.70) indicating very little role of clay minerals in fixation of these elements and instead, role of K-feldspar in HFSE fixation in these shales; whereas strong correlation of HFSEs with Al_2O_3 in the Rampur (0.75, 0.88 and 0.97) and the Rewa shales (0.65, 0.97 and 0.82) suggests fixation of HFSEs in clay minerals. Further, the concentration of transition trace elements (TTEs: Cr, Ni and V) in Vindhyan shales shows very low or negative correlation with Al_2O_3 indicating that TTEs too are not fixed in K-feldspar and K-rich clays. This trace element variation in Vindhyan shales indicate increased terrigenous detrital flux in the depositional basin during the deposition of Arangi and Bijaygarh shales compared to Koldaha, Rampur, Rewa and Sirbu shales.

4.3. REE geochemistry

The REE concentrations of lower and upper Vindhyan shales are given in Table 2. The REEs in fine grained sedimentary rocks are immobile in nature and act as a natural indicator of provenance (Taylor and McLennan, 1985). The total concentration of REEs (ΣREE) in six Vindhyan shales ranges from 115 to 450 ppm (averaging 219.71) and displays a positive correlation with Al_2O_3 (r = 0.59; n = 73), suggesting that REE composition in Vindhyan shales was not affected in the course of hydraulic sorting and chemical weathering (Basu et al., 2017). In particular, the Arangi shale contains higher SiO_2 (78–88 wt%) compared to the rest of the

Vindhyan shales and its REE concentration also remains the lowest (ΣREE = 129). This could possibly be because of dilution effect of quartz (Cullers, 2000).

The chondrite-normalized REE pattern of Vindhyan shales (Arangi, Koldaha, Rampur, Bijaygarh, Rewa and Sirbu shales) is presented in Fig. 4 (cf. Taylor and McLennan, 1985). The plot shows enriched LREE (La_{CN}/Sm_{CN} = 4.00), relatively flat HREE (Gd_{CN}/Yb_{CN} = 1.46) and negative europium anomaly (Eu/Eu* = 0.66). The chondrite-normalized average REE values are also compared with that of PAAS (Fig. 4). The values are either near similar or marginally enriched in majority of the shale succession except the Arangi shale that records a significantly low REE concentration. The ratios of light and heavy REEs (ΣLREE/ΣHREE), $(La/Sm)_{CN}$, $(Gd/Yb)_{CN}$ and Eu/Eu* are considered as effective indices to characterize sediment provenance and sedimentary environment (Taylor and Mclennan, 1985; Hu et al., 2020). Vindhyan shales exhibit significant enrichment of light REEs with ΣLREE/ΣHREE ratio ranging from 3.46 to 11.46 with an average of 8.83 and europium anomaly (Eu/Eu*) values ranging between 0.56 and 0.75 (Table 2). McLennan (1989), McLennan and Taylor (1991) noted higher $(Gd/Yb)_{CN}$ ratio within Archean crust with typical recorded values above 2.0 in fine grained sedimentary rocks, and common values of $(Gd/Yb)_{CN}$ between 1.0 and 2.0 in the Post-Archean sedimentary rocks. It is important to note that average $(Gd/Yb)_{CN}$ values of Vindhyan shales (Arangi shale = 1.61, n = 4; Koldaha Shale = 1.46, n = 21; Rampur Shale = 1.61, n = 10; Bijaygarh shale = 1.21, n = 07; Rewa Shale = 1.34, n = 7; and Sirbu shale = 1.47; n = 23) are consistent and less than 2.0 (Table 2).

4.4. TOC, organic elements and hydrocarbons

TOC and organic elemental (carbon, C; hydrogen, H; sulfur, S) contents of Vindhyan shales are given in Table 3. Arangi, Rampur and Bijaygarh shales are pyrite bearing black shale and record good to very good TOC values ranging from 0.93% to 8.44% with an average of 3.76%. In contrast, Koldaha shale (0.52–1.53%), Rewa shale (0.33–1.36%) and Sirbu shale (0.29–1.08%), though occasionally recording values greater than 1.0, are dominantly poor in TOC content. TOC values of black shales from Arangi, Koldaha, Rampur of lower Vindhyan and Bijaygarh shales of upper Vindhyan are also measured through Rock Eval and the same has been used for assessing hydrocarbons and related parameters. It may also be observed that hydrogen content in organic matter present within Vindhyan shales is extremely low. While Rampur, Rewa and Sirbu shales have yielded values below detection limit, very low values are recorded from the Arangi (0.77), Koldaha (0.40) and Bijaygarh shales (1.20). Low H content and extremely low H/C ratio (0.09–0.31) that is less than 0.8 rule out the possibility of categorizing Vindhyan organic matters as of 'Type-I' or 'Type-II' (sapropelic) in character and instead, suggest their humic nature (North, 1985). Except for Bijaygarh shale, all shale units exhibit very low sulfur content (0.46–0.91%). High sulfur content in the Bijaygarh shale, collected from the Amjhore area, is corroborated with occurrence of massive pyrite deposits (Guha, 1971; Sarkar et al., 2010).

The Rock Eval data for organic matters separated from black shale units of Arangi, Koldaha, Rampur and Bijaygarh shales are provided in Table 4. The thermally liberated hydrocarbon (S_1) values range from 0.01 to 0.18 mg HC/g rock (milligram hydrocarbon per gram of rock sample). Hydrocarbon from thermal cracking of the kerogen (S_2) shows values in the range of 0.04–0.47 mg HC/g rock. The T_{max}. (temperature of highest S_2 yield) ranges between 292 C and 607 C, though clustering of values noted at temperature less than 500 C with only three samples (RN-1, RN-3 and B-36) yielded values greater than 500 C. Commonly, hydrocarbons obtained through cracking of kerogen at up to 500 C give the residual hydrocarbon potential or amount still capable of being generated from the organic matter. The Hydrogen Index (HI) of

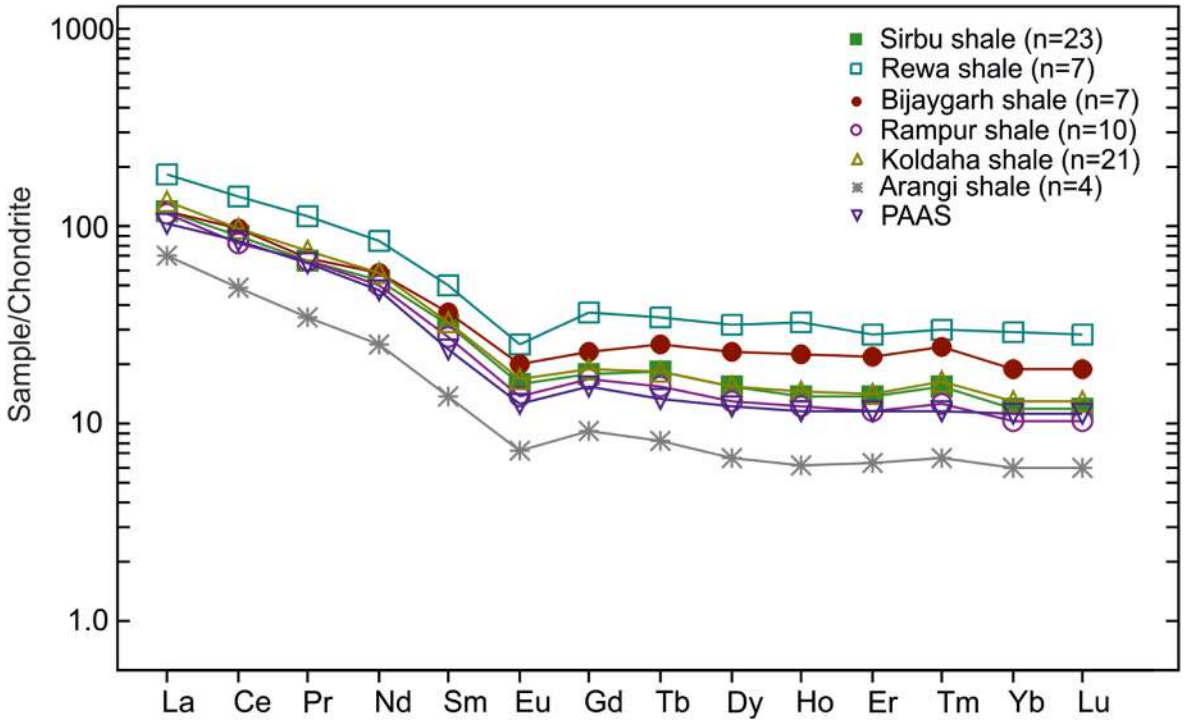

Fig. 4. Chondrite – normalized rare earth element (REE) pattern for Vindhyan shale samples. Note: Similarity in REE pattern for the shales from different stratigraphic levels, high LREE/HREE ratio, flat HREE pattern and measured negative Eu anomaly. PAAS (Taylor and McLennan, 1985) values are plotted for comparison.

Table 3
TOC and organic elemental (C, S and H) concentrations of Vindhyan shales.

Shale Formations	Range of TOC (%) value	Avg. Carbon (C)	Avg. Sulfur (S)	Avg. Hydrogen (H)
Sirbu shale	0.29 to 1.08 (n = 23)	1.38 (n = 6)	0.46 (n = 6)	bdl (n = 6)
Rewa shale	0.33 to 1.38 (n = 07)	1.62 (n = 3)	0.76 (n = 3)	bdl (n = 3)
Bijaygarh shale	2.82 to 3.36 (n = 07)	3.80 (n = 5)	13.53 (n = 5)	1.20 (n = 5)
Rampur shale	0.93 to 3.62 (n = 10)	4.47 (n = 6)	0.91 (n = 6)	bdl (n = 6)
Koldaha shale	0.52 to 1.33 (n = 21)	1.81 (n = 4)	0.84 (n = 4)	0.40 (n = 4)
Arangi shale	3.67 to 8.44 (n = 07)	7.87 (n = 4)	0.57(n = 4)	0.77 (n = 4)

bdl = below detection limit.

Table 4
Rock-Eval pyrolysis results of organic matters separated from Vindhyan shales showing T_{max}, Hydrogen Index (HI), and Oxygen Index (OI).

Sample	S_1	S_2	PI	T_{max}	S_3	TOC	HI	OI
Bijaygarh shale								
BGS-1	0.06	0.07	0.45	411	0.47	3.68	2	13
BGS-3	0.05	0.04	0.53	401	0.59	3.92	1	15
BGS-7	0.12	0.12	0.5	421	0.5	4.14	3	12
BGS-K-1	0.17	0.08	0.68	299	0.71	3.79	2	19
BGS-K-3	0.18	0.19	0.48	294	0.79	4.5	4	18
BGS-K-7	0.25	0.32	0.44	313	0.49	4.4	7	11
Rampur shale								
RN-4	0.05	0.05	0.53	294	0.71	1.06	5	67
RN-1	0.05	0.06	0.46	516	0.63	1.01	6	62
RN-3	0.01	0.04	0.25	519	0.55	0.98	7	65
RN-K-3	0.04	0.04	0.49	496	0.62	1.27	6	63
Koldaha shale								
KSK-1	0.05	0.04	0.58	306	0.16	0.09	44	178
KSK-2	0.06	0.03	0.64	292	0.16	0.09	33	178
KSK-3	0.01	0.02	0.38	452	0.1	0.12	40	175
Arangi shale								
B-31	0.07	0.26	0.2	481	2.11	10.43	5	28
B–K-30	0.18	0.41	0.31	474	2.28	8.13	5	28
B–K-33	0.4	0.37	0.52	309	2.13	4.55	8	47
B-36	0.05	0.08	0.38	607	1.44	8.01	1	18
B-30	0.11	0.47	0.19	480	2.41	10.14	5	24
B-33	0.06	0.06	0.51	299	3.37	4.91	1	69

studied Vindhyan shales range from 1 to 44 mg HC/g TOC whereas Oxygen Index (OI) varies between 11 and 178 mg HC/g TOC.

5. Discussion

5.1. Characteristics of provenance

On ternary discriminant diagram Al_2O_3-(CaO + Na_2O + K_2O)-(Fe_2O_3+MgO), most Vindhyan shales plot on illite line except the Bijaygarh shale samples which deviate marginally towards the (Fe_2O_3+MgO) apex (Fig. 5a) (cf. Hayashi et al., 1997). A weathered granitic source rock with strong control of clay minerals is suggested for most of the shale formations (cf. Cullers, 2000; Alvarez and Roser, 2007). Hayashi et al. (1997) proposed the Al_2O_3/TiO_2 ratio as an important indicator for provenance and suggested a range of 3–8 for mafic rocks, 8–21 for intermediate rocks and 21–70 for felsic rocks. Al_2O_3/TiO_2 ratios of Vindhyan shales display little difference (12–32 with an average of 23.19) and are distributed in the range of 'granite line' and within the field defined between granite and granodiorite lines, which is also corroborated in TiO_2 *vs.* Al_2O_3 binary diagram (Schieber, 1992) suggesting derivation of Vindhyan shales mostly from the felsic sources (Fig. 5b). The departure of Bijaygarh shale samples from the general trend is attributed to high diagenetic pyrite content (Guha, 1971; Sarkar et al., 2010) that causes its shift towards Fe_2O_3 axis in the Al_2O_3-(CaO + Na_2O + K_2O)-(Fe_2O_3+MgO) ternary plot and towards '3 granite + 1 basalt line' in the TiO_2 *vs.* Al_2O_3 binary diagram (Fig. 5a and b).

Besides absolute values, ratios between selected trace elements are also used for provenance characterization as they are characteristically different for felsic and mafic rocks. (Wronkiewicz and Condie, 1990; Cox et al., 1995; Nagarajan et al., 2007). Amongst these, the distinct difference in Th/Sc value between felsic (0.84–20.5) and mafic (0.05–0.22) rocks makes it a very useful proxy for provenance distinction (McLennan and Taylor, 1991). Th/Sc values of Vindhyan shales range from 0.25 to 3.64. Other elemental ratios, commonly used for provenance distinction, viz. Th/Co and La/Sc show values ranging from 0.18 to 8.03 and 1.54 to 9.86, respectively. On Th/Co *vs.* La/Sc bivariate plot, Vindhyan shales are plotted in the region of felsic source rocks (Fig. 5c) (Cullers, 2002; Basu et al., 2021). Supportive evidence is also obtained from La/Th *vs.* Hf binary diagram (Fig. 5d), in which Vindhyan shales occupy the field of felsic source region except for few samples from the Sirbu shale which bear signature for influx of older sediments (cf. Floyd and Leveridge, 1987). Furthermore, the consistent low values of Cr/Ni ratio (0.63–6.78) in all shale units of Vindhyan succession bear testimony for their derivation from felsic source(s) (Armstrong-Altrin et al., 2004; Nagarajan et al., 2007). This interpretation is well corroborated by trace elements proxy ratios such as La/Sc, Th/Sc, Th/Co, and Th/Cr (cf. Wronkiewicz and Condie, 1990; Cox et al., 1995; Cullers, 1995; Nagarajan et al., 2007). Th/Sc, Th/Co, Th/Cr, Cr/Th, and La/Sc ratios of shales are compared with signature values of these elemental ratios from felsic and mafic rocks (fine fraction) as well as within upper continental crust (UCC) and PAAS (Table 5). Cr/Th ratio of Vindhyan shales from all stratigraphic intervals record low values (2.55–8.73 with one value from Rampur Shale as high as 22.8) that fall largely within the range represented by felsic rocks (4.00–15.00) (Condie and Wronkiewicz, 1990). When average Cr/Th values recorded from shale units are compared with those of PAAS, it is observed that except for Sirbu shale (average ratio of 5.31), which has slightly lower Cr/Th ratio than that of PAAS (7.5), all other shale units have values strongly depleted with respect to the PAAS value (Table 5). In contrast to most shale formations, the small depletion in Cr/Th ratio within Sirbu shale is suggestive of relatively higher concentration of compatible element and bear signature of possible input from mafic component in the provenance.

Major and trace element-based interpretations also gain support from REE data. Relatively high LREE/HREE ratio with negative europium anomaly in Vindhyan shales is considered as a signature of felsic rocks in the source region which evolved through a history of plagioclase fractionation (Taylor and McLennan, 1985; Cullers, 1995; Manikyamba et al., 2008) (Fig. 4). On Eu/Eu* *vs.*$(Gd/Yb)_{CN}$ diagram (Fig. 6a), the Vindhyan samples largely plot in the field of Post-Archean rocks, below the $(Gd/Yb)_{CN}$ = 2.0 boundary and Eu/Eu* = 0.85 line with exception of one sample from Sirbu shale which plot very close to $(Gd/Yb)_{CN}$ ratio boundary (cf. McLennan and Taylor, 1991). This indicates incidence of intra-crustal differentiation processes on a regional scale in an overall felsic source terrain (Figs. 4 and 6a) (Gibbs et al., 1986; McLennan et al., 1989; Condie, 1993) with mixing of intermediate to mafic source only in

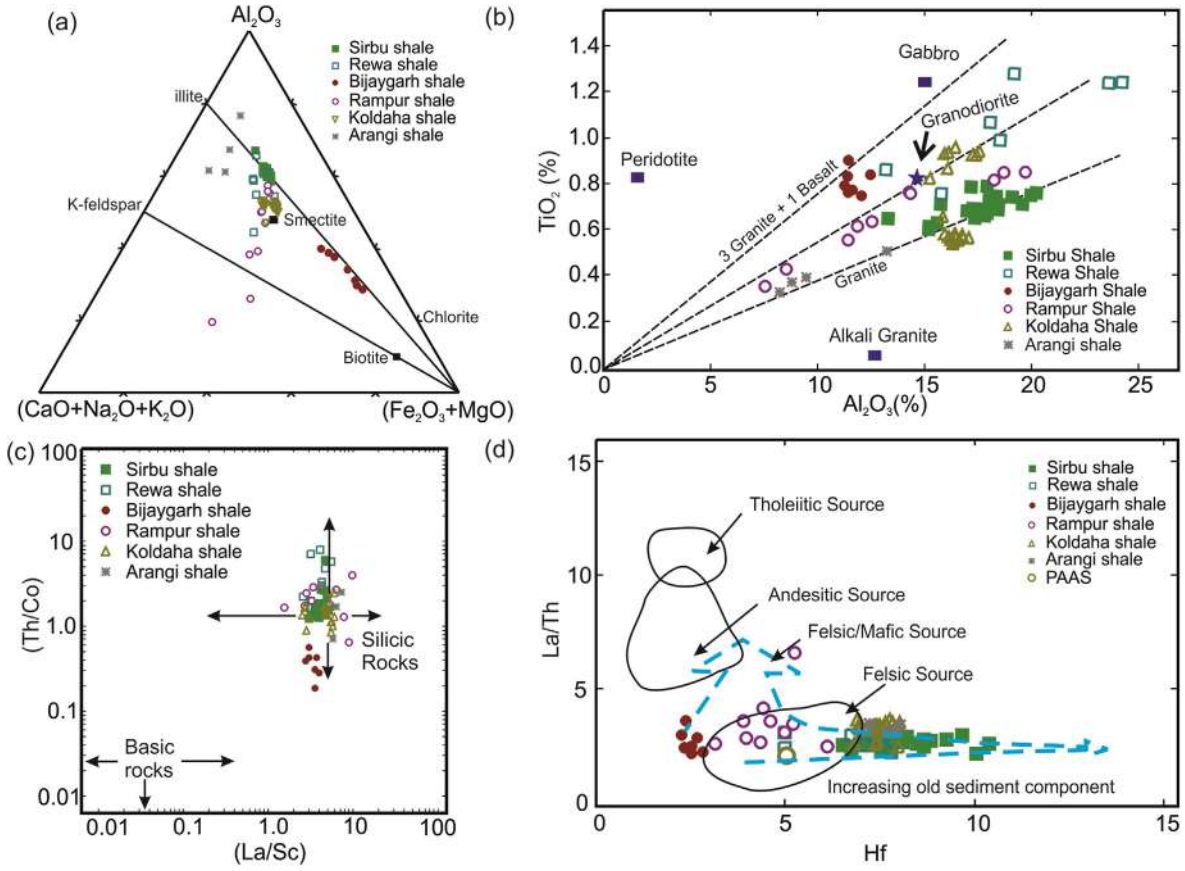

Fig. 5. (a) $Al_2O_3 - (CaO + Na_2O + K_2O) - (Fe_2O_3+MgO)$ ternary diagram showing plotting of Vindhyan shale samples. Note: Most of the samples are plotted from (Fe_2O_3+MgO) apex except Rampur and Bijaygarh Shale; (b) TiO_2–Al_2O_3 plot of Vindhyan shales with granite and 3 granite + 1 basalt trend line (after Schieber, 1992). Note: Most samples, except Bijaygarh Shale plot in the field defined by Granite and Granodiorite lines; (c) Th/Co vs. La/Sc plot for Vindhyan shales indicating their felsic source; (d) La/Th vs. Hf plot showing most of the Vindhyan samples falling in the felsic region except samples of Sirbu shale those depicting mixing of old sediment component.

Table 5
Trace element ratios of Vindhyan shales compared with ranges of ratios recorded from felsic and mafic rocks, UCC and PAAS compositions.

Elemental Ratios	Elemental ratios from shales of Vindhyan Supergroup					Range		Upper Continental Crust (UCC)	Post-Archean Australian Shale (PAAS)
	Sirbu shale	Rewa shale	Bijaygarh shale	Rampur shale	Koldaha shale	Felsic rocks	Mafic rocks		
Th/Sc	1.42-2.90	0.95-2.77	1.06-1.91	0.25-3.64	0.87-2.18	0.84-20.5	0.05-0.22	0.79	0.91
Th/Co	1.24-6.00	1.66-8.03	0.18-0.56	0.63-2.91	0.85-2.57	0.64-19.4	0.04-1.4	0.63	0.63
Th/Cr	0.11-0.26	0.11-0.39	0.16-0.30	0.04-0.17	0.11-0.33	0.13-2.7	0.018-0.046	0.13	0.13
Cr/Th	2.91-8.73	2.55-9.29	3.33-6.36	5.82-22.8	3.00–8.90	4.00–15.00	25–500	7.76	7.53
La/Sc	3.02–5.31	2.55-5.46	2.75-4.00	1.54-9.86	2.57-6.06	2.50-16.30	0.43-0.86	2.21	2.38

case of deposition of the Sirbu shale of upper Vindhyan.

Covering a large area in the north of Central Indian Tectonic Zone (CITZ), the Vindhyan Supergroup rocks in the Son valley overlie basement that consists of a number of geological provinces differing in terms of age and lithology. They include Bundelkhand granite, Bijawar Group, Gwalior Group, Chhotanagpur gneiss and Mahakoshal Group. Amongst these, the geological province that acted as active provenance for the basin has always remained speculative. Contradictory claims exist in literature regarding supply of Vindhyan detritus: some supported a provenance in the northern margin of the basin (Tandon et al., 1991) while others favoured supply from the southeastern margin of the basin (Chanda and Bhattacharyya, 1982; Soni et al., 1987). From disposition of facies belt and documentation of overwhelming northwesterly palaeocurrent direction irrespective of stratigraphic level, Bose et al. (2001) and Singh and Chakraborty (2020) suggested supply of sediments from southeastern margin of the Vindhyan Basin. From comparison of trace element and 'Nd' isotope data obtained from the Vindhyan succession and the Bundelkhand granite, Chakrabarti et al. (2007) ruled out the possibility of Bundelkhand granite as provenance for Vindhyan sediments. Taking into consideration i) overwhelming northwestward palaeocurrent, ii) geochemical signature of sediments matching closely to the upper crust, iii) types of clay minerals (illite + muscovite + smectite as subordinate) present within the Vindhyan argillaceous intervals (Paikaray et al., 2008), and iv) the chondrite normalized REEs of

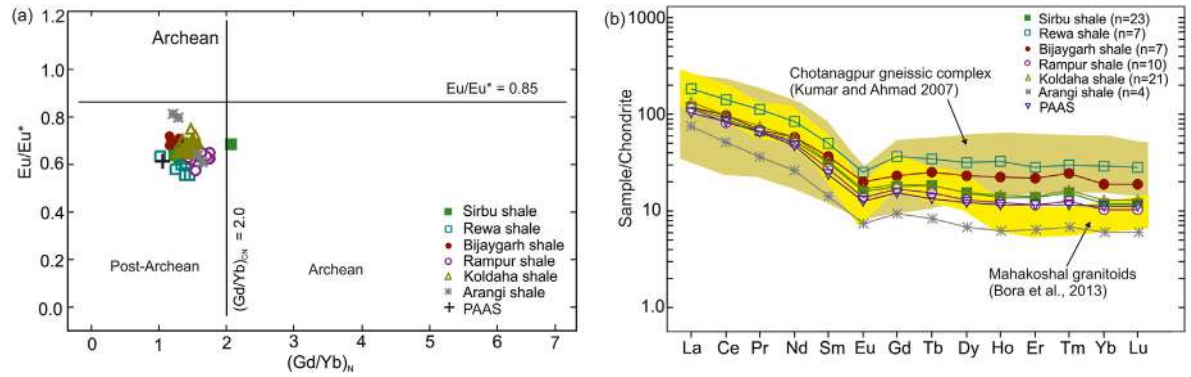

Fig. 6. (a) Plot of Eu/Eu* *vs.* $(Gd/Yb)_{CN}$ for Vindhyan shales. Fields are after McLennan and Taylor (1991); (b) Comparison of chondrite-normalized REE pattern of Vindhyan shales with that of Mahakoshal granitoids (Bora et al., 2013), Chhotanagpur gneissic complex (Kumar and Ahmad, 2007) and PAAS.

Vindhyan shales with that of Mahakoshals (Bora et al., 2013) and Chhotanagpur gneissic complex (CGC) (Kumar and Ahmad, 2007) (Fig. 6b), it is surmised that the CGC and Mahakoshal Group of rocks (with metasedimentaries and metavolcanics) present in the south and southeastern part of the basin acted as sources of sediments for the Vindhyan Basin. Granite, granodiorite with enclaves of tonalite and ultramafic suite of rocks in the CGC (Ramakrishnan and Vaidyanadhan, 2010) and presence of metabasic rocks and metasedimentaries in the basal part of Mahakoshal Group (Sleemanabad Formation) make them strong contender as provenance for Vindhyan sediments. The mixing of mafic source in the Sirbu shale might have resulted from tectonic uplift in the source area. Indeed, a continued tectono-thermal history is recorded from the E-W elongated CITZ at the southern and southeastern margins of the basin (Roy and Prasad, 2003; Paikaray et al., 2008; Mohanty, 2010). However, the inference can only be fully justified with a detail 'Nd' isotope mapping of all concerned geological provinces.

5.2. Provenance weathering and palaeoclimate

Nesbitt and Young (1982) proposed the CIA to quantify the extent to which sediments are subjected to chemical weathering in the source region and expressed it in a mathematical expression as:

$$CIA = Al_2O_3/ (Al_2O_3+CaO^*+Na_2O + K_2O)$$

Where CaO* is the amount of CaO incorporated in the silicate phase of the rock and all elements are in molecular proportion. Generally, the CIA values ranging from 50 to 65 indicate low chemical weathering with cold and dry climate; CIA values ranging between 65 and 85 suggest moderate chemical weathering with warm and humid climate; and values exceeding 85 indicate intense chemical weathering in a hot and humid climate (Nesbitt and Young, 1989; Hu et al., 2020).

The calculated CIA values of lower and upper Vindhyan shales are presented in Table 1. The lower Vindhyan shales have CIA values ranging between 59 and 79 with an average of 73, whereas in upper Vindhyan values are slightly higher ranging from 72 to 82 with an average of 79. The average CIA values of Vindhyan shales are higher than that of PAAS (CIA = 69) (Taylor and McLennan, 1985). Taking into consideration the K-metasomatism effect, CIA values of lower and upper Vindhyan shales are plotted in Al_2O_3–$(CaO^* + Na_2O)$–K_2O (A–CN–K) ternary diagram (Fig. 7) (Nesbitt and Young, 1984, 1989). After calibration, the CIA values for lower Vindhyan shales range from 75 to 90 with an average of 80 and upper Vindhyan shales between 85 and 100 with an average of 88 (Fig. 7). Except for the Rampur shale, data from the lower Vindhyan shales (Avg. corrected CIA = 80) show moderate scatter and incidence away from the A-K join. This indicates moderate degree of weathering in warm and humid climate. On the other hand, the upper Vindhyan shales record high corrected CIA values (85–100; Avg. 88) and suggest intense weathering condition with hot and humid climate in the provenance. The higher CIA values of Vindhyan shales (both lower and upper Vindhyan) in comparison to PAAS (69) suggest that weathering in the hinterland at the time of Vindhyan sedimentation had reached to a stage where Alkali and alkaline earth elements were actively removed from clay minerals (Taylor and McLennan, 1985).

Moreover, the elements Na, Ca and Sr are more depleted in the Vindhyan shales relative to PAAS than Al, Cs and Ba except for two samples of Rewa shale (PS4 and PS5). These depletions may be caused by two plausible processes. Firstly, the elements Ca and Sr reside in minerals that weather rapidly than those minerals which retain Al, Cs and Ba and thus, this depletion could be a result of weathering of source rock (cf. Roddaz et al., 2006). Secondly, such depletions may also be ascribed to parent rocks being depleted in plagioclase because both Ca and Sr are contained in plagioclase (Nesbitt and Young, 1984; Roddaz et al., 2006). Also, a consistent low value of CaO in Vindhyan shale relative to PAAS is suggestive of source being poor in plagioclase (Kasanzu et al., 2008).

5.3. Role of mineral sorting on shale composition

Sediment recycling and/or sorting can alter the abundance of specific elements and mineral composition of fine grained sedimentary rock. While Th/Sc is a sensitive indicator of source composition, Zr/Sc forms an important index of zircon enrichment in course of sediment transport and recycling. McLennan et al. (1993) used these contrasting characteristics for inference on effect of sedimentary processes like mineral sorting and zircon enrichment on sediment composition. On Th/Sc *vs.* Zr/Sc bivariate plot (Fig. 8), most Vindhyan shale samples plot near to average UCC and are sub-parallel to trend 1 indicating homogeneous composition and negligible influence of mineral sorting (McLennan et al., 2003; Manikyamba et al., 2008; Armstrong-Altrin et al., 2013). Only the Sirbu shale samples show a clear tendency to fall in line with trend 2 suggesting zircon addition/mixing during sediment sorting and recycling thereby corroborating influx of older sediments during Sirbu shale deposition (Fig. 5d). That there were periodic tectonic perturbations during the deposition of Koldaha and Sirbu shale successions got support from documentation of slumps and slide planes within these shale successions (Singh and Chakraborty, 2020). Furthermore, a few samples of Arangi and Koldaha shale fall between the two trends without showing any

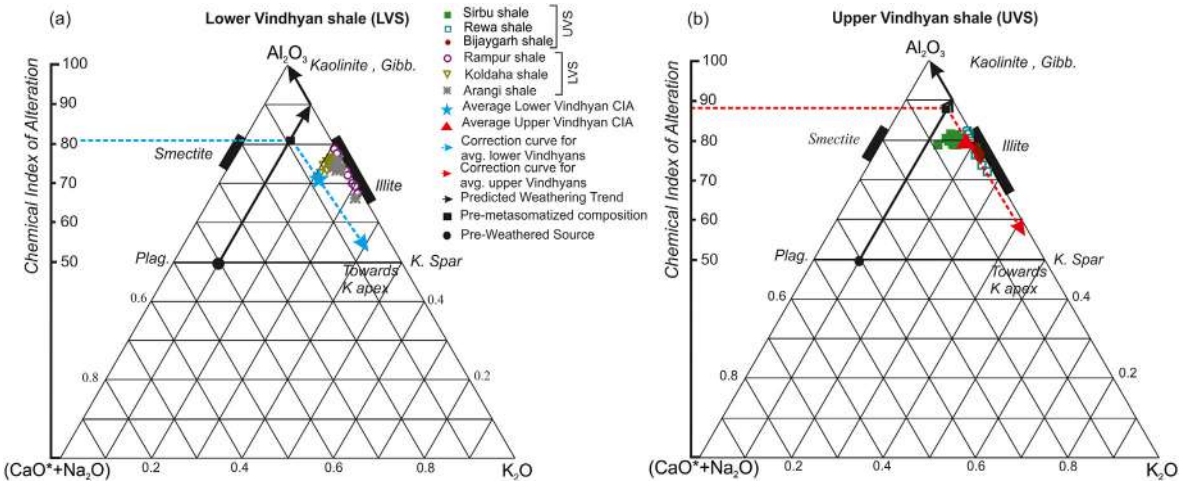

Fig. 7. A (Al_2O_3) −CN (CaO^*+ Na_2O) −K (K_2O) ternary diagram showing weathering trends for lower (a) and upper (b) Vindhyan shales (after Nesbitt and Young, 1982). While lower Vindhyan shales record corrected CIA value near to 80, the upper Vindhyan shales record values near to 88. Solid line arrow represents predicted weathering trend and dashed line arrow represents joining with K_2O apex.

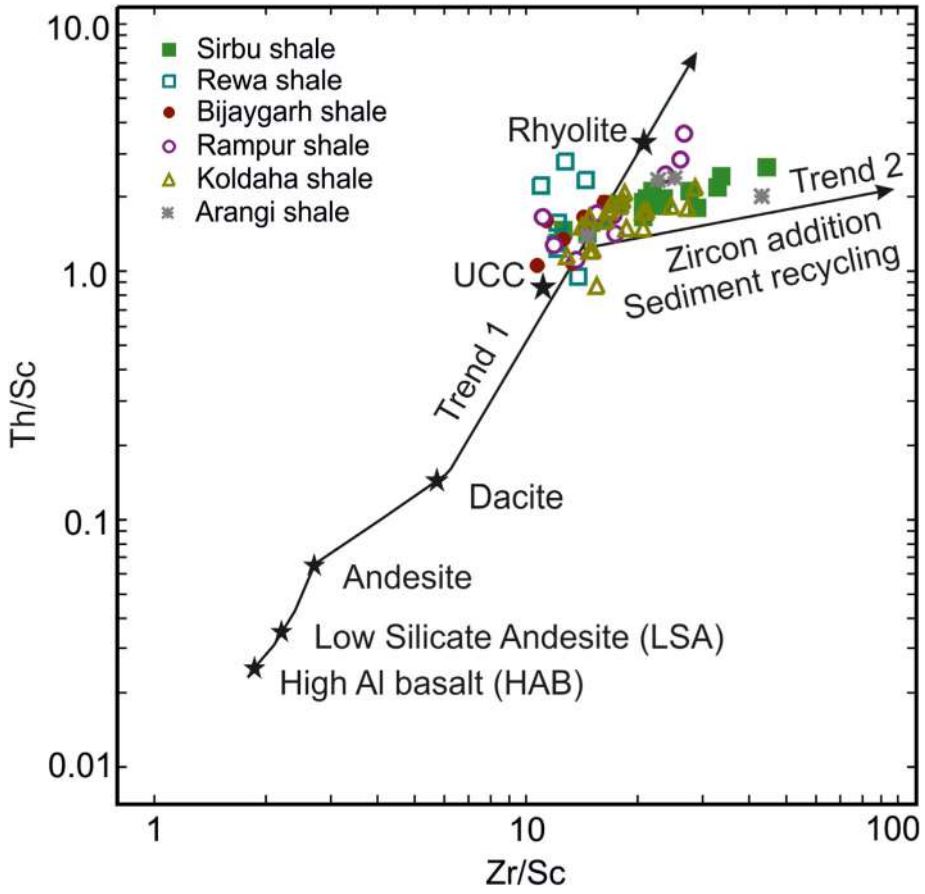

Fig. 8. Th/Sc *vs.* Zr/Sc bivariate plot (McLennan et al., 1993) for Vindhyan shale samples. Note: The zircon addition in Sirbu shale samples due to sediment sorting and recycling. UCC− Upper continental crust (Taylor and McLennan, 1985).

clear inclination to either trend; this tendency indicates a low to very low influence of mineral sorting in these samples. The idea is supported by a very poor correlation of trace elements with Al_2O_3 in the Koldaha shale ($Zr–Al_2O_3$, r = 0.10; $Nb–Al_2O_3$, r = 0.17 and $Ti–Al_2O_3$, r = 0.10) indicating that they are not fixed in clay minerals and may have supplied as detrital sediment (Kasanzu et al., 2008; Armstrong-Altrin et al., 2013).

5.4. Basin tectonics

For extrapolation of tectonic setting of the Vindhyan Basin, workers traditionally remained dependent on sediment

geochemistry (cf. Paikaray et al., 2008; Chakrabarti et al., 2007) and process-based physical sedimentology (Bose et al., 1997, 2001; Sarkar et al., 2002a; Chakraborty, 2006) in the absence or rare availability of high resolution geophysical data. The available tectonic models vary widely from an intracratonic setting (Chanda and Bhattacharyya, 1982; Soni et al., 1987), to a foreland setting (Chakrabarthy and Bhattacharyya, 1996; Chakrabarti et al., 2007; Shukla et al., 2020) to temporally evolved rift to sag setting (Bose et al., 1997, 2001; Sarkar et al., 2002b; Singh and Chakraborty, 2020). The tectonic settings deciphered using trace and rare earth elements (e.g. Th, Sc, Ti, Nb, and Zr) are considered reliable due to relatively low diagenetic mobility and low residence time of these elements in seawater (LaMaskin et al., 2008). On La/Y *vs.* Sc/Cr binary discrimination diagram (Fig. 9a), Vindhyan shales plot in the region of passive margin except for a few samples of Arangi and Rampur shale that show slightly higher ratio (Bhatia, 1985; Bhatia and Crook, 1986; McLennan and Taylor, 1991; McLennan et al., 1993; Armstrong-Altrin et al., 2013). The passive margin tectonic setting is also supported by REE patterns of Vindhyan shales, which record values similar to average PAAS values with significant negative europium anomaly (Eu/Eu* = 0.58 to 0.75) while the sediments of active continental margin show a fractionated REE patterns with wide range of negative Eu anomaly. However, Vindhyan shale samples plot in a wide range spanning from passive to active continental margin on (Th-Sc-Zr/10) and (Th–La-Sc) ternary diagrams (Fig. 9b and c) (McLennan et al., 1980). Though most Vindhyan samples fall in the fields of passive to active continental margin, a few samples of Koldaha and Rewa shales also occupy the continental island arc field (Fig. 9) (Shukla et al., 2020). The wide scatter of Vindhyan samples may be due to i) sorting effect of elements such as Th, Sc and Zr in the course of sediment transport history and ii) intermittent igneous activity in course of sedimentation (such as porcellanites in the Semri Group, kimberlite pipe in the Kaimur Formation, etc.). Plotting of most Bijaygarh shale samples near to boundary between passive margin and continental island arc field is possibly resulted from relatively low Sc (11–16 ppm), marginally higher La (48 ppm) and relatively high Zr/Th ratios (8.48–12.43). The high Zr/Th ratio and low Sc concentrations within the Bijaygarh shale indicate its recycled, passive margin character (Bhatia and Crook, 1986; Descourvieres et al., 2011).

Since the binary and ternary diagrams have limitations in discrimination between rift and foreland settings and have tendency for clustering of analytical data either in the field of active continental margin or in passive margin; tectonic interpretation from these data and plots often becomes inconclusive. Hence, relying on limited geochemical signature (Fig. 9) and process-based physical sedimentology from previous studies (Bose et al., 1997; Singh and Chakraborty, 2020), it is suggested that Vindhyan Basin initiated as a rift evolves into a sag basin with time (Bose et al., 2001; Singh and Chakraborty, 2020). Converging (both east- and west-ward) palaeocurrent, role of quartz in shale mineralogy and structural features such as slumps, slide planes, small scale listric faults within Koldaha shale, all indicate the basin was tectonically active in the form of extensional regional tectonics, thereby indicating a half-graben like situation (cf. Bose et al., 1997). From Rampur shale onward the role of tectonics became subdued, which is attested in well-developed facies gradient from proximal to distal part of the shelf (Singh and Chakraborty, 2020). With stability in tectonics, it is also logical that the climate started its domination on tectonics as weathering over erosion. This is attested by dominating role of clay minerals (illite + muscovite) from Rampur shale onward

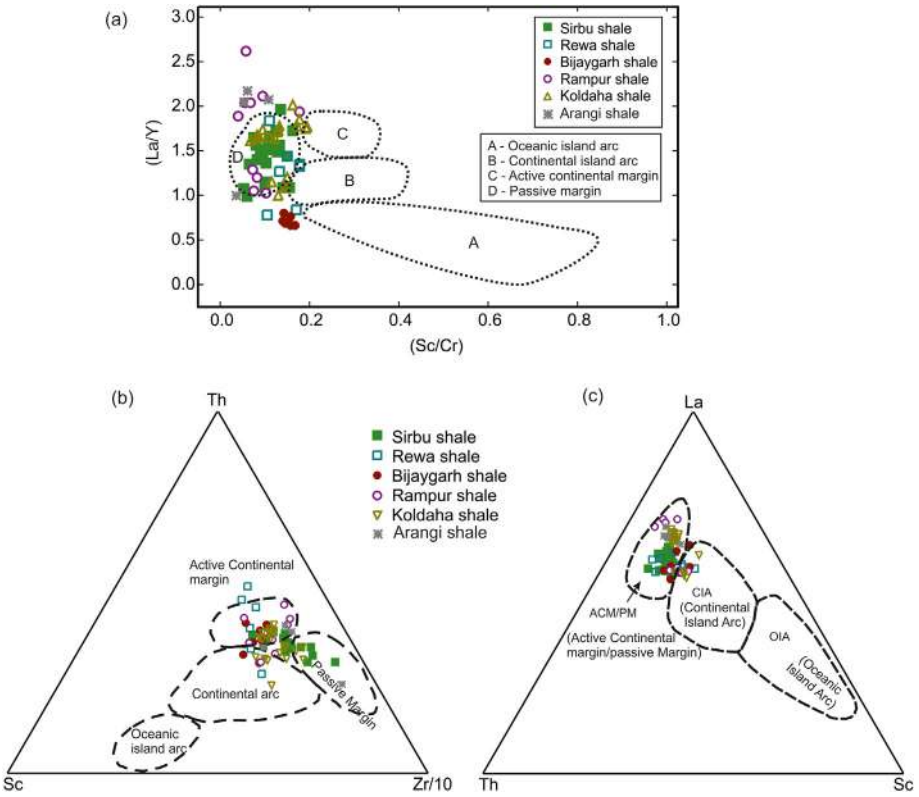

Fig. 9. (a) Sc/Cr *vs.* La/Y bivariate plot showing Vindhyan samples in the field of passive margin (after Bhatia and Crook, 1986); (b) The plotting of Vindhyan samples in Th-Sc-Zr/10 ternary diagram across the field ranging from passive margin to active continental margin; (c) La–Th-Sc ternary diagram (McLennan et al., 1980), too, plots Vindhyan samples in the field of active continental margin/passive margin (ACM/PM).

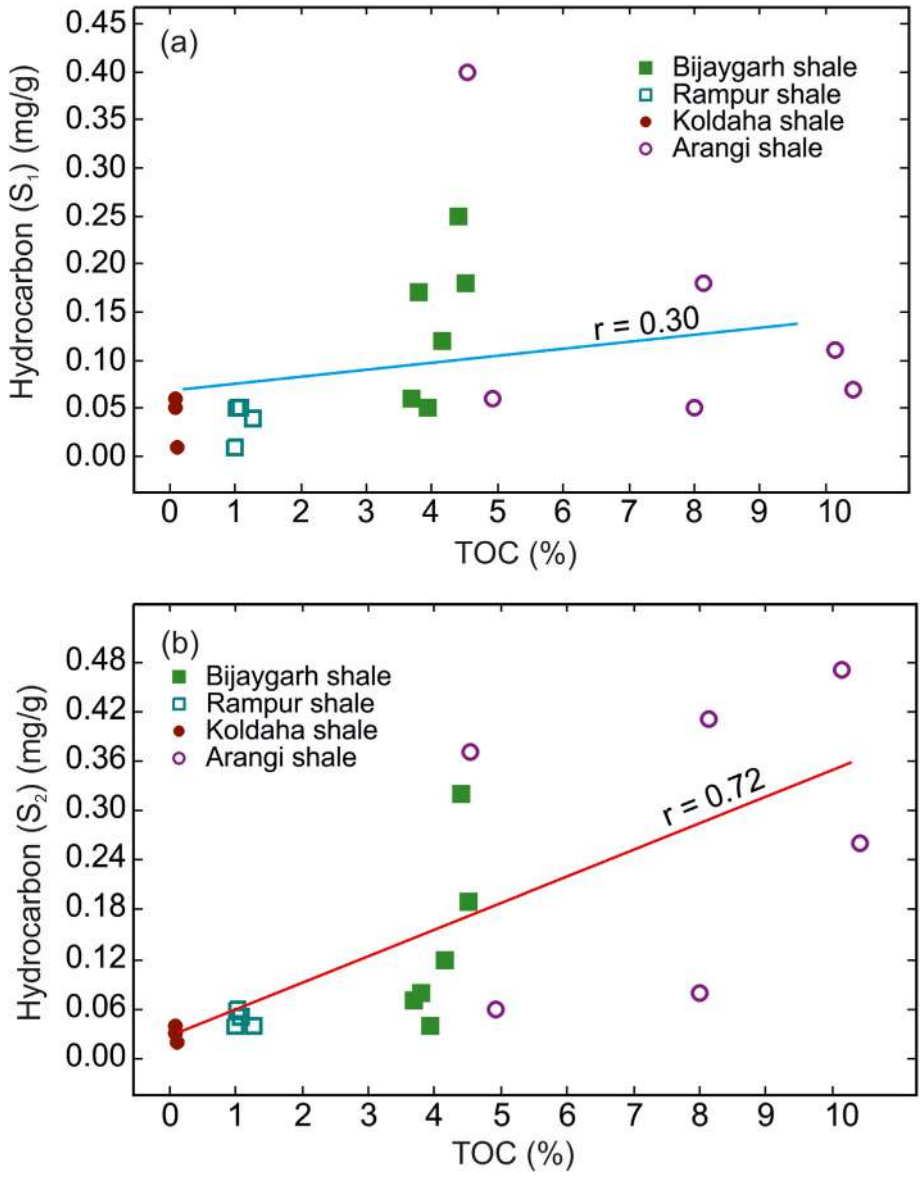

Fig. 10. Correlation of S_1 (thermally liberated hydrocarbon; mg HC/g rock) (a), and S_2 (hydrocarbon from cracking of kerogen; mg HC/g rock) (b), with TOC in shale samples of Vindhyan succession.

and higher CIA values in the provenance with time (Fig. 5a and b). Since the intracratonic set-up prevailed for a longer period, the basin received sediment from more and more deep rooted weathered provinces present within the stable craton (Roser and Korsch, 1986). The idea is also supported by dominant quartz arenitic character of upper Vindhyan sandstones (Chanda and Bhattacharyya, 1982; Bose et al., 2001; Sen et al., 2014).

5.5. Hydrocarbon source rock potential

The Rock Eval data from four Vindhyan black shales, namely Arangi, Koldaha, Rampur and Bijaygarh shales with high TOC contents (maximum of up to 10.43%), indicate presence of low to moderate S_1 and S_2 hydrocarbons. The hydrogen Index (HI = [S_2 x 100]/TOC) of samples is very low with majority of values < 10 mg HC/g TOC due to low H/C ratio and low S_2 hydrocarbon. CO_2 derived from organic matter in the course of heating in inert helium atmosphere is represented by S_3, which ranges from 0.1 to 3.37 mg CO_2/g rock (Table 4). In particular, the samples from Arangi shale (B-30, 31, 33, 36 and B–K-30, 33) yielded higher values (1.44–3.37 mg CO_2/g rock). The Oxygen Index (OI = [S_3 x 100]/TOC) is a parameter that correlates with O/C atomic ratio. The OI values (11–178 mg CO_2/g TOC) of Vindhyan shales are higher than their respective HI values (1–44 mg HC/g TOC). These data corroborate the idea drawn from C–H–S analyses that the organic matters in Vindhyan shales are richer in oxygen compared to hydrogen and hence, may be categorized as of Type-III (humic) variety.

Although the shale samples are very low in hydrogen (H) content, an attempt has been made to investigate the correlations of S_1 and S_2 with TOC. Fig. 10 demonstrates weak to moderate correlations of S_1 and S_2 with TOC for organic matters from the Arangi, Koldaha, Rampur and Bijaygarh shales. It may be noticed that while S_1 shows poor correlation (r = 0.30) with TOC (Fig. 10a), S_2 show moderate to good (r = 0.72) correlation (Fig. 10b). On closer inspection it can be seen that while samples from the Koldaha shale show very poor results on all counts. The Rampur shale shows

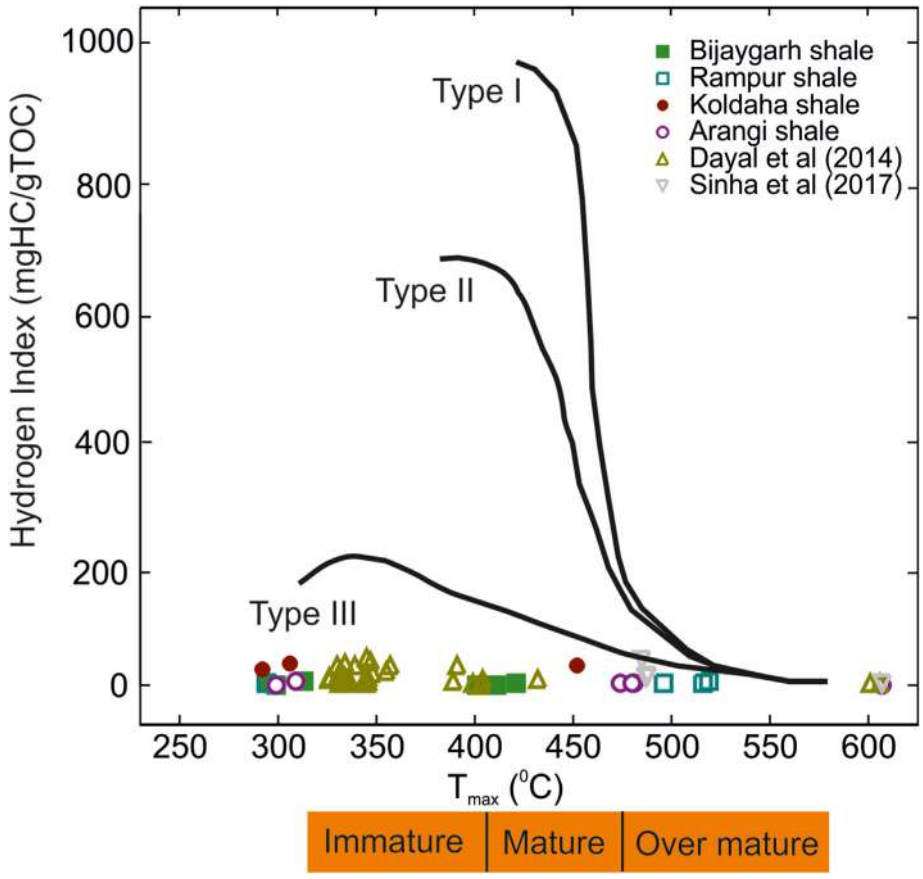

Fig. 11. Hydrogen Index (HI) *vs.* T_{max} (temperature of highest yield of S_2) plot of shales from Vindhyan Supergroup. Note: Few samples from Arangi and Bijaygarh Shale plot in the mature temperature range.

moderate TOC content (around 1%, a few showing more than 2%) and very poor S_1 and S_2 values, thereby ruling out any possibility as potential hydrocarbon source. In comparison, samples from the Arangi shale and Bijaygarh shale with higher TOC values (2.82–8.44) and wide range (low to moderate) of S_1 and S_2 values bear indication for hydrocarbon potential to certain extent (Table 3, Table 4).

Besides content and quality of organic matters, another major concern is its maturity as organic matters need to be properly cooked to yield hydrocarbon (North, 1985). To verify this, hydrogen indexes (HI) of shale samples are plotted against their respective T_{max} values in modified Van Krevelen diagram (Van Krevelen, 1961; Tissot and Welte, 1978; Hunt, 1996) (Fig. 11). Based on T_{max} values, organic matters are classified as immature, mature (oil window condition), transitional and over mature; while T_{max} value of less than 435 C is considered as thermally immature stage for organic matters, the temperatures of 435 C- 455 C, 455 C – 470 C and higher than 470 C, are considered as thermally mature, transitional and super mature stages, respectively (Tissot and Welte, 1978; Peters, 1986). Fig. 11 shows a wide variation in thermal maturity of organic matters from Vindhyan shales ranging from thermally immature to super mature. The Arangi samples show a wide range varying from immature to mature, whereas the Bijaygarh samples fall in the mature field, Koldaha samples plot in the immature field and Rampur shale samples commonly fall in super mature field. Samples from Bijaygarh shale and a few samples from the Arangi shale plot near mature field, indicating Type III character of kerogen. We have also observed that our samples from the Rampur shale plot in the super mature field and nearly coincide with samples described by Sinha et al. (2017) from the Arangi Formation. It may be due to low TOC content, differing sample character and differential sample location (Fig. 11). Also, we compared our Rock Eval data from the Bijaygarh shale with available Rohtas and Bijaygarh Formation data from Dayal et al. (2014) in order to get a comprehensive view on the thermal maturity of organic matters. Although organic matters from the Rohtas Formation, lower Vindhyan (Khachhuhar, Murlipahar and Banjari area) are recorded as thermally immature in character (Dayal et al., 2014), we found organic matters from samples of Bijaygarh shale (Amjhore area) and a few samples from the Arangi shale (Dalla area) thermally mature (Fig. 11). Incidentally, Dayal et al. (2014) also documented the same result from the Bijaygarh shale samples. This confirms Type III kerogen of gas-prone character for the organic matters present in Arangi and Bijaygarh shale units (Fig. 11). This is also supported by the fact that these shale units were deposited in shallow marine conditions with proliferation of microbialites and algal mat, and yield high TOC content (Sharma, 1996; Singh et al., 2018; Singh and Chakraborty, 2020). Therefore, combining the Rock Eval data and Van Krevelen bivariate analysis it can be inferred that both Arangi and Bijaygarh shales have good to very good gas generation potential.

Despite the long-held perception that the Precambrian rocks are not of high hydrocarbon potential simply because of their poor preservation potential and very low organic matter content, the present study highlights the importance of studying the long-neglected Precambrian sedimentary successions, particularly the Proterozoic successions, in terms of their hydrocarbon generation potential. Demarcation of stratigraphic levels in terms of the

sequestered Precambrian organic matters and studies related to characterization of organic matters including identification of constituent organic molecules and biomarkers will go a long way in understanding the teleconnection between atmosphere, hydrosphere and biosphere in the early evolution of planet Earth.

6. Conclusion

Shales of the Palaeo-Mesoproterozoic Vindhyan Basin are studied for whole rock inorganic and organic geochemistry to determine provenance, palaeoweathering condition, hydraulic sorting, tectonic setting and hydrocarbon source rock potential. The geochemical investigation suggests a derivation of detritus from felsic source(s) except for the Sirbu shale which bear signature of influx also from intermediate to mafic source. A comparative study of REEs demonstrates Mahakoshals and Chhotanagpur gneissic complex (CGC) as most probable source rock terrains for Vindhyan sediments. Most Vindhyan shales have homogeneous composition and limited influence of mineral sorting except for the Sirbu shale that has undergone sediment recycling and zircon enrichment. An evolution in climate and weathering condition is inferred through the Vindhyan depositional history with moderate degree of weathering in warm and humid climate during lower Vindhyan deposition that advanced to intense weathering conditions in a hot and humid climate during the deposition of the upper Vindhyan. The present study highlights the inadequacy in geochemistry-based tectonic discriminant diagrams for drawing inference on rift- or sag-related origin of any intracratonic basin such as the Vindhyan Basin. The organic matters of Vindhyan shales indicate its humic character and is categorized as a Type III variety based on poor hydrogen content, extremely low H/C ratio and higher oxygen index. A wide variation in thermal maturity of organic matters extending from immature to super mature stage is also noticed. Only the organic matters from Bijaygarh and Arangi shales fall near the mature field in modified Van Krevelen diagram (HI *vs.* T_{max}). Higher TOC, wide range of S_1 and S_2 hydrocarbon values and mature organic matters from these shale units indicate good to very good potential as gas source rocks.

Declaration of competing interest

The authors declare that they have no known competing financial interests or personal relationships that could have appeared to influence the work reported in this paper.

Acknowledgement

AKS is grateful to the director, Birbal Sahni Institute of Palaeosciences, Lucknow for providing necessary facilities and permission to publish this manuscript. PPC acknowledges funding from the Department of Science and Technology (DST#/SR/S4/ES-528/2010), New Delhi and infrastructural facility from Department of Geology, University of Delhi. Research funding from the Council of Scientific and Industrial Research (CSIR#09/045(1021)/2010-EMR-I) and the University of Delhi (Sch./UTA/2010/58053) is also gratefully acknowledged. We are also thankful to two anonymous reviewers for suggested revisions and valuable feedback that significantly improved this article.

References

Algeo, T.J., Tribovillard, N., 2009. Environmental analysis of paleoceanographic systems based on molybdenum–uranium covariation. Chem. Geol. 268, 211–225.

Alvarez, N.O., Roser, B.P., 2007. Geochemistry of black shales from the lower cretaceous paja formation, eastern cordillera, Colombia: source weathering, provenance and tectonic setting. J. South. Am. Earth. Sci. 23, 271–289.

Armstrong-Altrin, J.S., Lee, Y.I., Verma, S.P., Ramasamy, S., 2004. Geochemistry of sandstones from the Upper Miocene Kudankulam Formation, southern India: implications for provenance, weathering and tectonic setting. J. Sediment. Res. 74, 285–297.

Armstrong-Altrin, J.S., Nagarajan, R., Madhavaraju, J., Rosalez-Hoz, L., Lee, Y.I., Balaram, V., Cruz-Martínez, A., Avila-Ramírez, G., 2013. Geochemistry of the Jurassic and upper cretaceous shales from the Molango region, Hidalgo, eastern Mexico: implications for source-area weathering, provenance, and tectonic setting. Compt. Rendus Geosci. 345, 185–202.

Banerjee, S., Dutta, S., Paikaray, S., Mann, U., 2006. Stratigraphy, sedimentology and bulk organic geochemistry of black shales from the Proterozoic Vindhyan Supergroup (central India). J. Earth. Sys. Sci. 115, 37–48.

Basu, A., Bickford, M.E., 2015. An alternate perspective on the opening and closing of the intracratonic Purana basins in peninsular India. J. Geol. Soc. India 85, 5–25.

Basu, H., Dandele, P.S., Kumar, K.R., Achar, K.K., Umamaheswar, K., 2017. Geochemistry of black shales from the Mesoproterozoic Srisailam Formation, Cuddapah basin, India: implications for provenance, palaeoweathering, tectonics, and timing of Columbia breakup. Chem. Erde-Geochem 77, 596–613.

Basu, P., Banerjee, A., Chakrabarti, R., 2021. A combined geochemical, Nd, and stable Ca isotopic investigation of provenance, paleo-depositional setting and sub-basin connectivity of the Proterozoic Vindhyan Basin, India. Lithos 388, 106059.

Basu, S., Verchovsky, A.B., Bogush, A., Jones, A.P., Jourdan, A.L., 2019. Stability of organic carbon components in shale: implications for carbon cycle. Front. Earth Sci. 7, 297.

Bhatia, M.R., 1985. Rare earth element geochemistry of Australian Palaeozoic graywackes and mudrocks: provenance and tectonic control. Sediment. Geol. 45, 97–113.

Bhatia, M.R., Crook, K.A.W., 1986. Trace element characteristics of graywackes and tectonic setting discrimination of sedimentary basins. Contrib. Mineral. Petrol. 92, 181–193.

Blatt, H., 1985. Provenance studies and mudrocks. J. Sediment. Petrol. 55, 69–75.

Bora, S., Kumar, S., Yi, K., Kim, N., Lee, T.H., 2013. Geochemistry and U–Pb SHRIMP zircon chronology of granitoids and microgranular enclaves from Jhirgadandi pluton of Mahakoshal Belt, Central India Tectonic Zone, India. J. Asian Earth Sci. 70, 99–114.

Bose, P.K., Banerjee, S., Sarkar, S., 1997. Slope-controlled seismic deformation and tectonic framework of deposition: Koldaha Shale, India. Tectonophysics 269, 151–169.

Bose, P.K., Eriksson, P.G., Sarkar, S., Wright, D.T., Samanta, P., Mukhopadhyay, S., Mandal, S., Banerjee, S., Altermann, W., 2012. Sedimentation patterns during the Precambrian: a unique record? Mar. Petrol. Geol. 33, 34–68.

Bose, P.K., Sarkar, S., Chakraborty, S., Banerjee, S., 2001. Overview of the meso- to neo-proterozoic evolution of the Vindhyan Basin, central India. Sediment. Geol. 141, 395–419.

Bose, P.K., Sarkar, S., Das, N.G., Banerjee, S., Mandal, A., Chakraborty, N., 2015. Proterozoic Vindhyan Basin: configuration and evolution. Geol. Soc. London. Memoirs. 43, 85–102.

Chakrabarti, R., Basu, A.R., Chakrabarti, A., 2007. Trace and Nd-isotope evidence for sediments sources in the mid-Proterozoic Vindhyan Basin, central India. Precambrian Res. 159, 260–274.

Chakrabarthy, C., Bhattacharyya, A., 1996. The Vindhyan basin: an overview in the light of current perspectives. In: Bhattacharya, A. (Ed.), Recent Advances in Vindhyan Geology, vol. 36. Geological Society of India Memoir, pp. 301–312.

Chakraborty, P.P., 2004. Facies architecture and sequence development in a Neoproterozoic carbonate ramp: Lakheri Limestone member, Vindhyan Supergroup, central India. Precambrian Res. 132, 29–53.

Chakraborty, P.P., 2006. Outcrop signatures of relative sea level fall on a siliciclastic shelf: examples from the Rewa Group of Proterozoic Vindhyan basin. J. Earth. Syst. Sci. 115 (1), 23–36.

Chakraborty, P.P., Pant, N.C., Paul, P., 2015. Controls on sedimentation in Indian palaeoproterozoic basins: clues from the Gwalior and Bijawar basins, central India. Geol. Soc. London. Memoirs. 43, 67–83.

Chakraborty, P.P., Tandon, S.K., Roy, S.B., Saha, S., Paul, P.P., 2020. Proterozoic sedimentary basins of India. In: Gupta, N., Tandon, S. (Eds.), Geodynamics of the Indian Plate. Springer Geology, Springer, Cham, pp. 145–177.

Chanda, S.K., Bhattacharyya, A., 1982. Vindhyan sedimentation and paleogeography: Post-Auden developments. In: Valdiya, K.S., Bhatia, S.B., Gaur, V.K. (Eds.), Geology of Vindhyanchal. Hindusthan Publishing Corp., New Delhi, pp. 88–101.

Condie, K.C., 1993. Chemical composition and evolution of the upper continental crust: contrasting results from surface samples and shales. Chem. Geol. 104, 1–37.

Condie, K.C., Des Marais, D.J., Abbott, D., 2001. Precambrian superplumes and supercontinents: a record in black shales, carbon isotopes, and paleoclimates? Precambrian Res. 106, 239–260.

Condie, K.C., Wronkiewicz, D.J., 1990. A new look at the Archean–Proterozoic boundary: sediments and the tectonic setting constraint. In: Naqvi, S.M. (Ed.), Precambrian Continental Crust and its Economic Resources. Elsevier, Amsterdam, pp. 61–84.

Cox, R., Lowe, D.R., Cullers, R.L., 1995. The influence of sediment recycling and basement composition of evolution of mudrock chemistry in the southwestern United States. Geochem. Cosmochim. Acta 59, 2919–2940.

Cozzi, A., Rea, G., Craig, J., 2012. From global geology to hydrocarbon exploration: Pakistan and Oman Ediacaran-Early Cambrian petroleum plays of India. In: Bhat, G., Craig, J., Thurow, J.W., Thusu, B., Cozzi, A. (Eds.), Geology and

Hydrocarbon Potential of Neoproterozoic–Cambrian Basins in Asia, vol. 366. Geological Society, London, Special Publications, pp. 131–162.
Craig, J., Biffi, U., Galimberti, R.F., Ghori, K.A.R., Gorter, J.D., Hakhoo, N., Le Heron, D.P., Thurow, J., Vecoli, M., 2013. The palaeobiology and geochemistry of Precambrian hydrocarbon source rocks. Mar. Petrol. Geol. 40, 1–47.
Crawford, A.R., Compston, W., 1970. The age of the Vindhyan system of Peninsular India. J. Geol. Soc. London. 125, 351–371.
Cullers, R.L., 1995. The controls on the major-and trace-element evolution of shales, siltstones and sandstones of Ordovician to Tertiary age in the Wet Mountains region. Colorado, USA: Chem. Geol. 123, 107–131.
Cullers, R.L., 2000. The geochemistry of shales, siltstones and sandstones of Pennsylvanian-Permian age, Colorado, USA: implications for provenance and metamorphic studies. Lithos 51, 181–203.
Cullers, R.L., 2002. Implications of elemental concentrations for provenance, redox conditions, and metamorphic studies of shales and limestones near Pueblo, CO, USA. Chem. Geol. 191, 305–327.
Dayal, A.M., Mani, D., Madhavi, T., Kavitha, S., Kalpana, M.S., Patil, D.J., Sharma, M., 2014. Organic geochemistry of the Vindhyan sediments: implications for hydrocarbons. J. Asian Earth Sci. 91, 329–338.
Deru, X., Xuexiang, G., Pengchun, L., Guanghao, C., Bin, X., Bachlinski, R., Zhuanli, H., Gonggu, F., 2007. Mesoproterozoic-Neoproterozoic transition: geochemistry, provenance and tectonic setting of clastic sedimentary rocks on the SE margin of the Yangtze Block, South China. J. Asian Earth Sci. 29, 637–650.
Descourvieres, C., Douglas, G., Leyland, L., Hartog, N., Prommer, H., 2011. Geochemical reconstruction of the provenance, weathering and deposition of detrital-dominated sediments in the Perth Basin: the Cretaceous Leederville Formation, south-west Australia. Sediment. Geol. 236, 62–76.
Dutta, S., Steiner, M., Banerjee, S., Erdtmann, B.D., Jeevankumar, S., Mann, U., 2006. Chuaria circularis from the early Mesoproterozoic Suket Shale, Vindhyan Supergroup, India: insights from light and electron microscopy and pyrolysis-gas chromatography. J. Earth. Sys. Sci. 115, 99–112.
Eriksson, P.G., Mazumder, R., Sarkar, S., Bose, P.K., Altermann, W.V., Van der Merwe, R., 1999. The 2.7–2.0 Ga volcano-sedimentary record of Africa, India and Australia: evidence for global and local changes in sea level and continental freeboard. Precambrian Res. 97, 269–302.
Floyd, P.A., Leveridge, B.E., 1987. Tectonic environment of the Devonian mode and geochemical evidence from turbiditic sandstones. J. Geol. Soc. 144, 531–542.
Fu, X., Wang, J., Zeng, Y., Tan, F., Feng, X., 2010. REE geochemistry of marine oil shale from the Changshe Mountain area, northern Tibet, China. Int. J. Coal Geol. 81, 191–199.
Ghosh, S.K., Negi, M., Jalal, P., Sinha, S., 2016. Proterozoic sedimentary successions in the Himalayan Orogen: Stratigraphy, sedimentology and palaeobasinal conditions. Himal. Geol. 37, 121–140.
Gibbs, A.K., Montgomery, D.W., O'Day, P.A., Erslev, E.A., 1986. The Archean–Proterozoic transition: evidence from geochemistry of metasedimentary rocks of Guyana and Montana. Geochem. Cosmochim. Acta 50, 2125–2141.
Guha, J., 1971. Sulfer isotope study of pyrite deposit of Amjhore, Shahbad District, Bihar, India. Econ. Geol. 66, 326–330.
Hayashi, K., Fujisawa, H., Holland, H.D., Ohmoto, H., 1997. Geochemistry of 1.9 Ga sedimentary rocks from northeastern Labrador, Canada. Geochem. Cosmochim. Acta 61, 4115–4137.
Herron, M.M., 1988. Geochemical classification of terrigeneous sands and shales from core or log data. J. Sediment. Petrol. 58, 820–829.
Hunt, J.M., 1996. Petroleum Geochemistry and Geology, second ed. W.H. Freeman and Company, San Francisco.
Hu, S., Wang, K., Wang, T., Yang, T., Luo, P., Shi, S., Wang, S., Su, J., 2020. Sedimentary environment and organic matter accumulation of Neoproterozoic black shale in the North China Craton: a case study of the Tonian Baishugou Formation in the Luonan area. Palaeogeogr. Palaeoclimatol. Palaeoecol. 547, 109694.
Kasanzu, C., Maboko, M.A., Manya, S., 2008. Geochemistry of fine-grained clastic sedimentary rocks of the Neoproterozoic Ikorongo Group, NE Tanzania: implications for provenance and source rock weathering. Precambrian Res. 164, 201–213.
Krishnan, M.S., 1968. Geology of India and Burma. Tata McGraw Hill Publication, New Delhi.
Krishnan, M.S., Swaminath, J., 1959. The Great Vindhyan Basin of northern India. J. Geol. Soc. 1, 10–36.
Kumar, A., Ahmad, T., 2007. Geochemistry of mafic dykes in part of Chotanagpur gneissic complex: petrogenetic and tectonic implications. Geochem. J. 41, 173–186.
Lafargue, E., Marquis, F., Pillot, D., 1998. Rock-Eval 6 applications in hydrocarbon exploration, production, and soil contamination studies. Rev. l'Instit. Franc. Pet. 53, 421–437.
LaMaskin, T.A., Dorsey, R., Vervoort, J.D., 2008. Tectonic controls on mudrock geochemistry, Mesozoic rocks of eastern Oregon and western Idaho, USA: implications for Cordilleran tectonics. J. Sediment. Res. 78, 765–783.
Li, D., Chen, Y., Wang, Z., Lin, Y., Zhou, J., 2012. Paleozoic sedimentary record of the Xing-Meng orogenic belt, Inner Mongolia: implications for the provenances and tectonic evolution of the central Asian orogenic belt. Chin. Sci. Bull. 57, 776–785.
Malone, S.J., Meert, J.G., Banerjee, D.M., Pandit, M.K., Tamrat, E., Kamenov, G.D., Pradhan, V.R., Sohl, L.E., 2008. Paleomagnetism and detrital zircon geochronology of the upper Vindhyan sequence, Son valley and Rajasthan, India: a ca. 1000 Ma closure age for the purana basins? Precambrian Res. 164, 137–159.
Mandal, S., Choudhuri, A., Mondal, I., Sarkar, S., Chakraborty, P.P., Banerjee, S., 2019. Revisiting the boundary between the lower and upper Vindhyan, Son Valley, India. J. Earth. Sys. Sci. 128, 1–16.
Manikyamba, C., Kerrich, R., Gonzalez-Alvarez, I., Mathur, R., Khanna, T.C., 2008. Geochemistry of Paleoproterozoic black shales from the Intracontinental Cuddapah basin, India: implications for provenance, tectonic setting, and weathering intensity. Precambrian Res. 162, 424–440.
Mazumder, R., Bose, P.K., Sarkar, S., 2000. A commentary on the tectono sedimentary record of the pre-2.0 Ga continental growth of India vis-a-vis a possible pre-Gondwana Afro-Indian subcontinent. J. Afr. Earth Sci. 30, 201–217.
McLennan, S.M., 1989. Rare earth elements in sedimentary rocks: influence of provenance and sedimentary processes. In: Lipin, B.R., McKay, G.A. (Eds.), Geochemistry and Mineralogy of Rare Earth Elements. Reviews in Mineralogy, vol. 21. Mineralogical Society of America, Chantilly, pp. 169–200.
McLennan, S.M., Bock, B., Hemming, S.R., Hurowitz, J.A., Lev, S.M., 2003. The roles of provenance and sedimentary processes in the geochemistry of sedimentary rocks. In: Lenz, D.R. (Ed.), Geochemistry of Sediments and Sedimentary Rocks: Evolutionary Considerations to Mineral Deposit-forming Environments, vol. 4. Geological Association of Canada, GeoText, pp. 7–31.
McLennan, S.M., Hemming, S., McDaniel, D.K., Hanson, G.N., 1993. Geochemical approaches to sedimentation, provenance and tectonics. In: Johnson, M.J., Basu, A. (Eds.), Processes Controlling the Composition of Clastic Sediments. Geological Society of America, Special Paper, USA, pp. 21–40.
McLennan, S.M., McCulloch, M.T., Taylor, S.R., Maynard, J.B., 1989. Effects of sedimentary sorting on neodymium isotopes in deep-sea turbidites. Nature 337, 547–549.
McLennan, S.M., Nance, W.B., Taylor, S.R., 1980. Rare earth element -thorium correlation in sedimentary rocks and composition of continental crust. Geochem. Cosmochim. Acta 44, 1833–1839.
McLennan, S.M., Taylor, S.R., 1991. Sedimentary rocks and crustal evolution: tectonic setting and secular trends. J. Geol. 99, 1–21.
Meert, J.G., Pandit, M.K., Pradhan, V.R., Banks, J., Sirianni, R., Stroud, M., Newstead, B., Gifford, J., 2010. Precambrian crustal evolution of Peninsular India: a 3.0 billion year odyssey. J. Asian Earth Sci. 39, 483–515.
Mohanty, S., 2010. Tectonic evolution of the Satpura Mountain Belt: a critical evaluation and implication on supercontinent assembly. J. Asian Earth Sci. 39, 516–526.
Mondal, M.E.A., Goswami, J.N., Deomurari, M.P., Sharma, K.K., 2002. Ion microprobe $^{207}Pb/^{206}Pb$ ages of zircons from the Bundelkhand Massif, northern India: implications for crustal evolution of the Bundelkhand–Aravalli supercontinent. Precambrian Res. 117, 85–100.
Nagarajan, R., Armstrong-Altrin, J.S., Nagendra, R., Madhavaraju, J., Moutte, J., 2007. Petrography and geochemistry of terrigenous sedimentary rocks in the Neoproterozoic Rabanpalli Formation, Bhima Basin, Southern India: implications for paleoweathering condition, provenance, and source rock composition. J. Geol. Soc. India 70, 297–312.
Nesbitt, H.W., Young, G.M., 1982. Early Proterozoic climates and plate motions inferred from major element chemistry of lutites. Nature 299, 715–717.
Nesbitt, H.W., Young, G.M., 1984. Prediction of some weathering trends of plutonic and volcanic rocks based on thermodynamic and kinetic considerations. Geochem. Cosmochim. Acta 48, 1523–1534.
Nesbitt, H.W., Young, G.M., 1989. Formation and diagenesis of weathering profiles. J. Geol. 97, 129–147.
North, F.K., 1985. Petroleum Geology. Allen and Unwin, London.
Ohta, T., 2004. Geochemistry of Jurassic to earliest Cretaceous deposits in the Nagato Basin, SW Japan: implication of factor analysis to sorting effects and provenance signatures. Sediment. Geol. 171, 159–180.
Paikaray, S., Banerjee, S., Mukherji, S., 2008. Geochemistry of shales from the paleoproterozoic to neoproterozoic Vindhyan Supergroup: implications on provenance, tectonics and paleoweathering. J. Asian Earth Sci. 32, 34–48.
Patranabis-Deb, S., 2004. Lithostratigraphy of the Neoproterozoic Chhattisgarh sequence: it's bearing on the tectonics and paleogeography. Gondwana Res. 7, 323–337.
Peters, K., 1986. Guidelines for evaluating petroleum source rocks using programmed pyrolysis. Am. Assoc. Petr. Geol. 70, 318–329.
Ramakrishnan, M., Vaidyanadhan, R., 2010. Geology of India. Geological Society of India, Bangalore.
Ray, J.S., Martin, M.W., Veizer, J., Bowring, S.A., 2002. U–Pb zircon dating and Sr isotope systematics of the Vindhyan Supergroup, India. Geology 30, 131–134.
Raza, M., Dayal, A.M., Khan, A., Bhardwaj, V.R., Rais, S., 2010. Geochemistry of lower Vindhyan clastic sedimentary rocks of Northwestern Indian shield: implications for composition and weathering history of Proterozoic continental crust. J. Asian Earth Sci. 39, 51–61.
Raza, M., Khan, A., Bhardwaj, V.R., Rais, S., 2012. Geochemistry of Mesoproterozoic sedimentary rocks of upper Vindhyan Group, southeastern Rajasthan and implications for weathering history, composition and tectonic setting of continental crust in the northern part of Indian shield. J. Asian Earth Sci. 48, 160–172.
Roddaz, M., Viers, J., Brusset, S., Baby, P., Boucayrand, C., Hérail, G., 2006. Controls on weathering and provenance in the Amazonian foreland basin: insights from major and trace element geochemistry of Neogene Amazonian sediments. Chem. Geol. 226, 31–65.
Roser, B.P., Korsch, R.J., 1986. Determination of tectonic settings of sandstone-mudstone suits using SiO_2 content and K_2O/Na_2O ratio. J. Geol. 94, 635–650.
Roser, B.P., Korsch, R.J., 1988. Provenance signatures of sandstone-mudstone suites determined using discriminant function analysis of major-element data. Chem.

Geol. 67, 119–139.
Roy, A.B., 1988. Stratigraphic and tectonic framework of the Aravalli mountain range. In: Roy, A.B. (Ed.), Precambrian of the Aravalli Mountain, Rajasthan, India. Geological Society of India, Memoir, vol. 7, pp. 3–32.
Roy, A., Prasad, M.H., 2003. Tectonothermal events in central Indian tectonic Zone (CITZ) and its implications in Rodinian crustal assembly. J. Asian Earth Sci. 22, 115–129.
Roy, P., Balaram, V., Kumar, A., Satyanarayanan, M., Gnaneshwar Rao, T., 2007. New REE and trace Element data on two international kimberlitic reference materials by ICP-MS. J. Geostand. Geoanalyt. Res. 31, 261–273.
Saini, N.K., Mukherjee, P.K., Rathi, M.S., et al., 1998. A new geochemical reference sample of granite (DG-H) from Dalhousie, Himachal Himalaya. J. Geol. Soc. India 52, 603–606.
Sarkar, A., Chakraborty, P.P., Mishra, B., Bera, M.K., Sanyal, P., Paul, S., 2010. Mesoproterozoic sulphidic ocean, delayed oxygenation and evolution of early life: sulphur isotope clues from Indian Proterozoic basins. Geol. Mag. 147, 206–218.
Sarkar, S., Banerjee, S., Chakraborty, S., Bose, P.K., 2002a. Shelf storm flow dynamics: insight from the mesoproterozoic Rampur shale, central India. Sediment. Geol. 147, 89–104.
Sarkar, S., Chakraborty, S., Banerjee, S., Bose, P.K., 2002b. Facies sequence and cryptic imprint of sag tectonics in late Proterozoic Sirbu Shale, central India. In: Altermann, W., Corcoran, P. (Eds.), Precambrian Sedimentary Environments: A Modern Approach to Ancient Depositional Systems, vol. 33. International Association of Sedimentologists, Special Publication, pp. 369–382.
Schieber, J., 1992. A combined petrographical-geochemical provenance study of the Newland Formation, Mid-Proterozoic of Montana. Geol. Mag. 129, 223–237.
Schieber, J., 2011. Reverse engineering mother nature—shale sedimentology from an experimental perspective. Sediment. Geol. 238, 1–22.
Sen, S., Mishra, M., Patranabis-Deb, S., 2014. Petrological study of the Kaimur Group sediments, Vindhyan Supergroup, Central India: implications for provenance and tectonics. Geosci. J. 18, 307–324.
Sharma, M., 1996. Microbialites (Stromatolites) from the Meso-Proterozoic Salkhan Limestone, Semri Group, Rohtas, Bihar: Their Systematics and Significance, vol. 36. Geological society of India, Memoir, pp. 167–196.
Sharma, M., Mishra, S., Dutta, S., Banerjee, S., Shukla, Y., 2009. On the affinity of Chuaria–Tawuia complex: a multidisciplinary study. Precambrian Res. 173, 123–136.
Sharma, M., Shukla, Y., 2009. Taxonomy and affinity of early Mesoproterozoic megascopic helically coiled and related fossils from the Rohtas Formation, the Vindhyan Supergroup, India. Precambrian Res. 173, 105–122.
Shukla, A.D., George, B.G., Ray, J.S., 2020. Evolution of the proterozoic Vindhyan Basin, Rajasthan, India: insights from geochemical provenance of siliciclastic sediments. Int. Geol. Rev. 62, 153–167.
Singh, A.K., Chakraborty, P.P., 2020. Shales of palaeo-mesoproterozoic Vindhyan Basin, central India: insight into sedimentation dynamics of proterozoic shelf. Geol. Mag. 1–22.
Singh, A.K., Chakraborty, P.P., Sarkar, S., 2018. Redox structure of Vindhyan hydrosphere: clues from total organic carbon, transition metal (Mo, Cr) concentrations and stable isotope (delta C-13) chemistry. Curr. Sci. 115, 1334–1341.
Sinha, H.N., Preety, K., Rai, P., Mohanty, D., Sarangi, S., 2017. The petroleum potential of the Arangi and Kajrahat limestone formations from the Semri Group, chopan, Uttar Pradesh, India. GeoResJ 13, 59–65.
Soni, M.K., Chakraborty, S., Jain, V.K., 1987. Vindhyan Supergroup – a review. In: Purana Basins of Peninsular India (Middle to Late Proterozoic). Geological Society of India, Memoir, vol. 6, pp. 87–138.
Tandon, S.K., Pant, C.C., Casshyap, S.M., 1991. Sedimentary Basins of India-Tectonic Context. Gyanodaya Prakashan, Nainital.
Taylor, S.R., McLennan, S.M., 1985. The Continental Crust: its Composition and Evolution. Blackwell Scientific Publications, Oxford.
Tissot, B.P., Welte, D.H., 1978. Petroleum Formation and Occurrence. A New Approach to Oil and Gas Exploration. Springer-Verlag, Berlin.
Trabucho-Alexandre, J., 2015. Organic matter-rich shale depositional environments. In: Rezaee, R. (Ed.), Fundamentals of Gas Shale Reservoirs. Wiley, New York, pp. 21–46.
Tyson, R.V., 2004. Variation in marine total organic carbon through the type Kimmeridge clay formation (late Jurassic). Dorset. UK. J. Geol. Soc. London. 161, 667–673.
Van Krevelen, D.W., 1961. Coal: Typology-Chemistry-Physics-Constitution. Elsevier Publishing Company, Amsterdam.
Verma, R.K., 1991. Geodynamic of the Indian Peninsula and Indian Plate Margins. A. A. Balkema, Rotterdam.
Wani, H., Mondal, M.E.A., 2011. Evaluation of provenance, tectonic setting and paleoredox conditions of the Meso-Neoproterozoic basins of the Bastar craton, Central Indian Shield: using petrography of sandstones and geochemistry of shales. Lithosphere 3, 143–154.
Wignall, P.B., 1994. Black Shales. Oxford University Press, New York, USA.
Wronkiewicz, D.J., Condie, K.C., 1987. Geochemistry of Archean shales from the Witwatersrand Supergroup, South Africa: source-area weathering and provenance. Geochem. Cosmochim. Acta 51, 2401–2416.
Wronkiewicz, D.J., Condie, K.C., 1990. Geochemistry and mineralogy of sediments from the ventersdorp and transvaal supergroups, South Africa: cratonic evolution during the early proterozoic. Geochem. Cosmochim. Acta 54, 343–354.
Zhu, G., Du, D., Chen, W., Sun, Q., Li, T., Zhang, Z., Chen, Z., 2018. Discovery of Precambrian thick black mudstones and its implication for hydrocarbon exploration in the southwest Tarim Basin. Petrol. Res. 3, 124–131.